International Journal of Advanced Materials Research
Vol. 4, No. 1, 2018, pp. 1-23
http://www.aiscience.org/journal/ijamr
ISSN: 2381-6805 (Print); ISSN: 2381-6813 (Online)

Unified Exact Solutions to the Hyperbolically Tapered Pressurized/Rotating Disks Made of Nonhomogeneous Isotropic/Orthotropic Materials

Vebil Yıldırım*

Mechanical Engineering Department, University of Çukurova, Adana, Turkey

Abstract

This work focuses mainly on the proposing closed-form solutions for the elastic fields in a power-law graded polar orthotropic hyperbolically tapered disk under separate inner/outer pressures, and centrifugal forces due to the rotation at a constant angular speed based on the present unified formulation. These formulas are capable of exact determination of the elastic behaviour of continuously hyperbolically tapered disks made of a single isotropic material, or made of a single polar orthotropic material, or made of a nonhomogeneous material formed by functionally power-law graded two isotropic materials, or a nonhomogeneous material formed by functionally power-law graded two orthotropic materials. Due to their multipurpose use, the present formulas may be directly employed in the material tailoring problems of hyperbolic disks. Three boundary conditions are studied: a disk with traction-free surfaces, a disk mounted on a circular rigid shaft having a traction-free outer surface, and a disk mounted on a circular rigid shaft having a rigid casing at the outer surface. The fibers are assumed to be reinforced along either radial (RR) or circumferential (CR) directions. After validating the present analytical solutions with both analytical and numerical results in the open literature, a comprehensive dimensionless parametric study is conducted to inspect of the effects of fiber orientations, profile parameters, inhomogeneity indexes, and boundary conditions under both pressure and centrifugal forces. It is chiefly revealed that the response of the disk having either CR-aligned or RR-aligned fibers may differ regarding to the mechanical loads. Some numerical results are presented in tabular forms.

Keywords

Variable-thickness Disk, Non-uniform Disk, Exact Solution, Functionally Graded, Polar Orthotropic, Circumferentially Aligned

Received: February 28, 2018 / Accepted: March 22, 2018 / Published online: June 6, 2018

1. Introduction

Rotating disks have been used commonly as turbine rotors, compressors, flywheels, disk brakes, gears, computer disk drives, and etc. They may be manufactured by either conventional or advanced isotropic and anisotropic materials with the purpose of withstanding much higher critical/burst speeds.

References [1-24] all focused on the derivation of closed-form solutions of stress and displacements in a rotating disk made of ordinary anisotropic materials. Among these, Murthy and Sherbourne [2], Reddy and Srinath [3], Gurushankar [7], Zenkour and Allam [18], and Eraslan et al. [23] studied variable-thickness orthotropic disks.

Advanced materials may have non-homogeneous material properties exhibiting either isotropic or anisotropic behaviour. From those, low-cost functionally graded (FG) metal-ceramic materials are in the class of nonhomogeneous isotropic advanced materials. Based on a chosen material

* Corresponding author
E-mail address: vebil@cu.edu.tr

grading rule, material properties vary continuously along one or more certain directions in FG metal-ceramics.

A simple power material grading rule [25-32], or an exponential grading rule [33, 38] were used to get closed-form solutions to the disks made of FG isotropic materials. From those, Horgan and Chan [25] and Nejad et al. [36] considered uniform disks subjected to the internal and external pressures while Yıldırım [31] studied pressure loads for hyperbolic disks. The others [26-30, 32-35, 37-38] studied with disks under just rotation.

Some of studies related to the elastic analysis of variable thickness disks were focused on the disks made of isotropic and homogeneous materials [35, 39-42]. Vivio and Vullo [43-44] just considered the density variation along the radial coordinate of the variable-thickness disk.

Here some studies which are in the scope of the present study: Apatay and Eraslan [45], and Eraslan and Akış [46] worked on the elastic analysis of parabolically-varying thickness disks made of FG-isotropic materials. By dividing the variable-thickness disk into sub-domains with uniform thickness, Bayat et al. [28] proposed a semi-analytical elastic solution for axisymmetric rotating hollow parabolic and hyperbolic disks. On the basis of a semi-exact method of Liao's homotopy analysis, Hassani et al. [47] studied elastic behaviour of rotating FG- isotropic hyperbolic rotating disks under different boundary conditions. Yıldırım's [30] formulation of the exact elastic response of a power-law graded hyperbolic rotating disk encompassed both continuously variations of elasticity modulus and material density including continuously variation of the thickness of the disk except variation of Poisson's ratios. Contrary to the literature all effects affecting the elastic behaviour of the disk with varying thickness such as internal and external pressures including rotation at a constant angular velocity were all studied under four physical boundary conditions and presented in compact forms in Yıldırım's study [30]. Yıldırım [31] further conducted a parametric study for hyperbolic thickness disks subjected to the pressure loads. Based on the both complementary functions and transfer matrix methods, Yıldırım and Kacar [48] introduced a versatile computer package program for the elastic analysis of FG-isotropic thick-walled annular structures, namely disks, cylinders, and spheres. Gang [32] analytically studied the stress analysis of a simple-power law graded hyperbolic rotating disk under stress-free conditions for four convergent disk profiles and negative inhomogeneity indexes. Recently, Yıldırım [49] also presented a comprehensive parametric study for a power-law graded hyperbolic rotating disk.

In quest of searching more advanced materials, scholars have begun to apply anisotropic materials, which exhibit different behaviours in tension, compression, and bending, as FG material constituents to form both anisotropic and inhomogeneous structures. As may be easily guessed, this types of materials are in the class of nonhomogeneous anisotropic advanced materials.

There are, unfortunately, a limited number of works on FG disks composed of anisotropic materials in the open literature [50-58]. Among these, Durodola and Attia [50] studied deformation and stresses in rotating hollow uniform disks made from FG orthotropic materials. Chen et al. [51] offered a 3-D analytical solution for a uniform rotating disk made of exponentially FG materials with transverse isotropy. Nie et al. [52] focused on the tailoring of elastic moduli in the radial direction to design a fiber-reinforced orthotropic linear elastic rotating disk with constant radial or hoop stress or constant in-plane shear stress. For a solid disk made of an orthotropic material, Nie et al.[52] gave explicit expressions for the required variations of the elastic moduli with the radius to attain a given state of stress. For a rotating annular CR-disk composed of a fiber-reinforced composite, the required radial variation of the volume fraction of fibers was calculated numerically and exhibited graphically by Nie et al. [52]. Kansal and Parvez [53] conducted a stress analysis on orthotropic graded rotating annular disks subjected to parabolic temperature distributions. Lubarda [54] analytically and numerically studied the elastic response of a uniformly pressurized cylindrically anisotropic hollow uniform thin rotating disks by using both the finite difference method and a Fredholm integral equation. Fredholm integral equation was also employed by Peng and Li [55] to consider FG hollow polar-orthotropic rotating disk under free-free and fixed-free boundary conditions. Kacar and Yıldırım [56] offered analytical formulas for the displacement and stress determination in power-law graded polar orthotropic uniform rotating disks under three boundary conditions. After deriving a confluent hypergeometric differential equation, Essa and Argeso [57] developed analytical solutions for the analysis of elastic polar orthotropic FG annular free-free and fixed-free disks rotating with constant angular velocity to study the effects of the anisotropy degree on the elastic fields. Essa and Argeso [57] considered a disk profile function as a product of a constant parameter, an exponential function of radial coordinate, r, and a power function of r similar to the variation of the other elastic properties. It is worth noting that Essa and Argeso [57] considered only centrifugal force effects on the elastic behaviour of non-uniform disks with radially aligned (RR) fibers. Based on the finite difference method and Voigt mixture grading rule with powers, Zheng et al. [58] numerically studied displacement and stress fields in a fiber-matrix FG variable thickness circumferentially aligned (CR) disk mounted on a rotating shaft and subjected to an angular deceleration. This study [58] revealed that disk deceleration has no effect on the radial and hoop stresses except

the shear stress.

As seen from the open literature that FG polar orthotropic disks subjected to the pressure loads are considered only by Lubarda [54] under the uniform disk assumption. Moreover there are just two studies conducted by References Essa and Argeso [57] and Zheng et al. [58] on the variable-thickness FG polar orthotropic rotating disks, and two studies conducted by Lubarda [54] and Zheng et al. [58] on the variable-thickness FG polar orthotropic rotating disks with circumferentially aligned fibers (CR) (Figure 1). This was a motivation of the author.

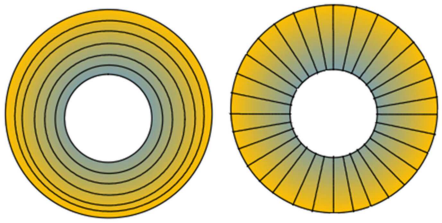

Figure 1. CR and RR disks, respectively.

As far as the author knows, the differential advantages of the present work over the available literature are, now, may be outlined as follows: i) Closed form formulas are presented only for FG polar orthotropic hyperbolic disks based on the Cauchi-Euler differential equation solution method. These formulas do, therefore, not contain any extra terms, ii) Present formulation may answer to various linear elastic axisymmetric disk problems under both pressure and centrifugal forces. Present closed-form formulas are, therefore, versatile. Disks made of many kind of materials such as a single isotropic and homogeneous material, a single polar orthotropic material, a power-law graded non-homogeneous-isotropic material, and a power-law graded nonhomogeneous polar orthotropic material may be studied without labouring, iii) The present formulas also originally include mounted-cased rotating disks as an additional boundary condition along with free-free and fixed-free surfaces, iv) Analytical formulas are originally developed for the elastic behaviour of traction free hyperbolic disks subjected to both the internal and external pressures in the present study, v) The present study also includes a comprehensive parametric study to inspect the effects of the gradient parameters which control the radial variation of the material properties, disk profile parameters which control the variation of the thickness along the radial coordinate, boundary conditions, loading types, and more originally the radially aligned (RR) and circumferentially aligned (CR) fiber orientations (Figure 1), vi) During the validation process, some of the test examples are also broadened to get an accurate common idea for such disks, vi) Some numerical results of fresh examples are also presented to serve as benchmark solutions to the scholars.

2. Formulation and Solution

By assuming axisymmetric small deformations, the strain-displacement relations in polar coordinates, (r,θ), are reduced to

$$\varepsilon_r(r)=\frac{du_r(r)}{dr},\qquad \varepsilon_\theta(r)=\frac{u_r(r)}{r} \tag{1}$$

where $\varepsilon_r(r)$ and $\varepsilon_\theta(r)$ are the radial and circumferential strains, while $u_r(r)$ is the radial displacement along the radial direction, r. The compatibility equation reads

$$\frac{d}{dr}(r\varepsilon_\theta(r))-\varepsilon_r(r)=0 \tag{2}$$

For linear elastic polar orthotropic materials, the constitutive equations describing relations between stresses and strains under plane stress assumption for thin plates are defined by Hooke's law as

$$\begin{aligned}\sigma_r(r)&=-\frac{E_\theta(r)\nu_{r\theta}}{\nu_{\theta r}(\nu_{r\theta}\nu_{\theta r}-1)}\varepsilon_r(r)-\frac{E_\theta(r)\nu_{r\theta}}{(\nu_{r\theta}\nu_{\theta r}-1)}\varepsilon_\theta(r)\\&=C_{11}(r)\varepsilon_r(r)+C_{12}(r)\varepsilon_\theta(r)\end{aligned} \tag{3}$$

$$\begin{aligned}\sigma_\theta(r)&=-\frac{E_\theta(r)\nu_{r\theta}}{(\nu_{r\theta}\nu_{\theta r}-1)}\varepsilon_r(r)-\frac{E_\theta(r)}{(\nu_{r\theta}\nu_{\theta r}-1)}\varepsilon_\theta(r)\\&=C_{12}(r)\varepsilon_r(r)+C_{22}(r)\varepsilon_\theta(r)\end{aligned} \tag{4}$$

where $E_r(r)$ and $E_\theta(r)$ are Young's moduli along the radial and circumferential directions, respectively. The radial and hoop stresses are denoted by $\sigma_r(r)$ and $\sigma_\theta(r)$ in the above equations. This equation is for the disks with radially aligned fibers (RR-disks) in which the material principal axes are defined by $1=r$, $2=\theta$, $3=z$. For the alignments in circumferential directions (CR-disks), $2=r$, $1=\theta$, $3=z$ is to be considered (Figure 1). Poisson's ratios are not independent from each other, they should obey Maxwell relation, $E_\theta(r)\nu_{r\theta}=E_r(r)\nu_{\theta r}$. It may be noted that the ratio of $E_\theta(r)$ to $E_r(r)$ defines the anisotropy/polar degree of the disk anisotropic material.

Equation of equilibrium in the radial direction under the centrifugal forces with a constant angular velocity, ω, is

$$\frac{1}{h(r)}\frac{d}{dr}\left(rh(r)\sigma_r(r)\right)-\sigma_\theta(r)=-\rho(r)\omega^2 r \tag{5}$$

where the material density and disk profile function are represented by $\rho(r)$ and $h(r)$, respectively. Equilibrium equation may be written as follows by making use of Eqs. (1), (3) and (4)

$$\left(\frac{d^2u_r(r)}{dr^2}+\frac{du_r(r)}{dr}\left(\frac{1}{r}+\frac{\frac{dC_{11}(r)}{dr}}{C_{11}(r)}+\frac{\frac{dh(r)}{dr}}{h(r)}\right)\right.$$
$$\left.+u_r(r)\left(-\frac{C_{22}(r)}{r^2C_{11}(r)}+\frac{C_{12}(r)}{rC_{11}(r)}\left(\frac{\frac{dC_{11}(r)}{dr}}{C_{11}(r)}+\frac{\frac{dh(r)}{dr}}{h(r)}\right)\right)\right)=-\frac{\rho(r)\omega^2 r}{C_{11}(r)} \quad (6)$$

This is a second order differential equation called Navier equation with variable coefficients. It governs the elasto-static behaviour of non-uniform disks made of any arbitrarily continuously graded polar orthotropic materials. The non-uniform disk may be in any form of various disk profiles as long as the plain stress assumption for thin plates is preserved.

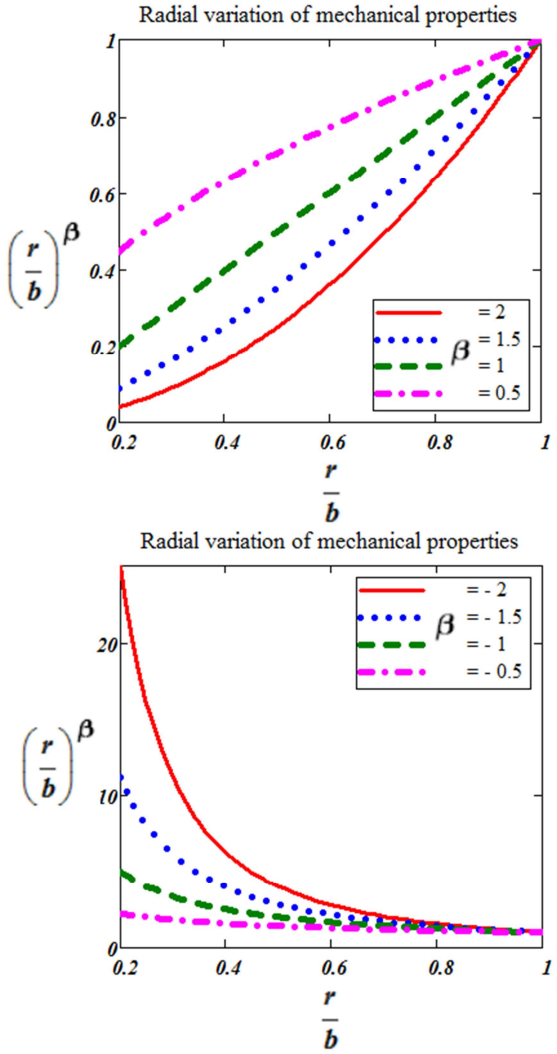

Figure 2. Variation of elastic properties for $(a/b)=0.2$.

By employing some special types of continuous functions, it is possible to get analytical solutions to the problem as stated in Introduction. A simple power rule is one of the well-known one, which is frequently used to get Navier equation with constant coefficients. In the present study, elasticity moduli, thickness and material density variations are all assumed to obey a simple power law as in Eqs. (7) and (8) (Figures 2-3).

$$E_r(r)=E_r^b\left(\frac{r}{b}\right)^{\beta_1},\quad E_\theta(r)=E_\theta^b\left(\frac{r}{b}\right)^{\beta_1} \quad (7)$$

$$\rho(r)=\rho^b\left(\frac{r}{b}\right)^{\beta_1},\quad h(r)=h_o\left(\frac{r}{b}\right)^{\beta_3} \quad (8)$$

where a and b are the radii of the inner and outer surfaces of the disk, respectively; β_1 and β_2 are the inhomogeneity parameters while β_3 is the disk profile parameter whose sign and value controls the profile shape of the disk (Figure 3); h_o is the reference thickness. As being a superscript in Eqs. (7) and 8, b represents the corresponding material property at the outer surface.

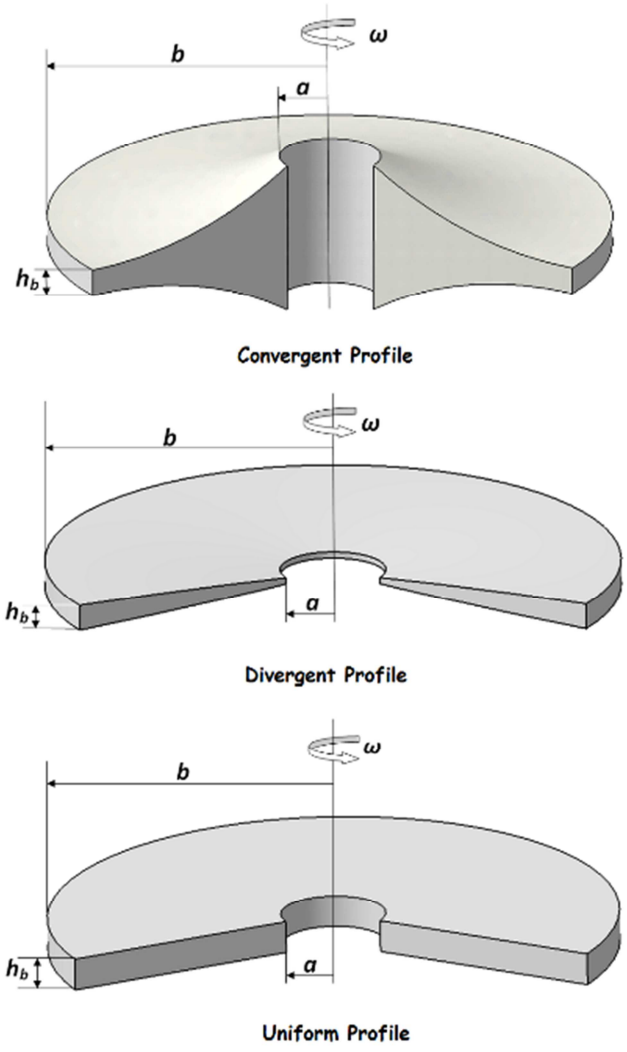

Figure 3. Disk profiles.

Figure 3 shows the general appearance of both the divergent ($\beta_3 > 0$) and convergent ($\beta_3 < 0$) profile types of the disk. $\beta_3 = 0$ overlaps the uniform disk profiles. $\beta_3 = 1$ gives a linear profile.

The nonlinear terms either β_1 or β_2 in Eqs. (7) and (8) may behave as shown in Figure 2 regarding to their signs and values. Positive inhomogeneity indexes suggest an increase in the property from the inner surface to the outer. A relatively sharp increase may be observed for higher values of the index. A positive index also means much reinforced outer surface than the inner. For negative inhomogeneity indexes, the inner surface become much more considerable stiff than the outer. It is worth noting that those increases/decreases directly depend on the aspect ratio (a/b). Since the disks have the highest aspect ratios compared to the cylinders and spheres, higher negative inhomogeneity indexes may present implausible solutions. Due to this reason, some investigations have considered just the local application of the simple power rule for disk type structures. In FG polar orthotropic disk problems, Voigt rule of the power of volume fractions of the constituents is indeed more plausible material rule to be applied in such analyses [55, 58]. However, it is almost impossible to get analytical solutions without making further assumptions to the problem with it. In such cases, employment of some numerical solution techniques which present reliable solutions becomes compulsory for even for the simplest problem. Despite those, the urgent necessity of some simple closed-form solutions has given a motivation to the present study. The present study is, therefore, expected to be able to meet some demands of the related industry and academics, and to get an idea about the main problem.

Convergent and divergent disk profiles considered in the present study are illustrated in Figure 4 for $(a/b) = 0.2$ and $h_o = a$ to make visible the differences between the profiles.

It may be noted that only β_3 has a contribution to the governing equation. Hence the chosen of h_o becomes optional. The final geometry of the disk may, hence, be modified by using different h_o values.

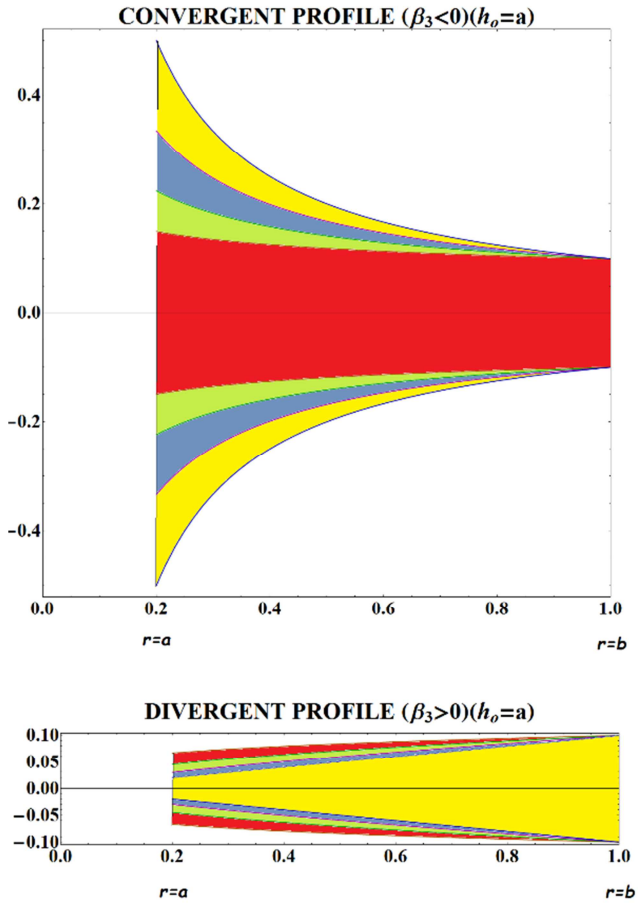

Figure 4. Convergent and divergent disk profiles considered for $h_o = a = 0.2$ $(\beta_3 = -1, -0.75, -0.5, -0.25, 0, 0.25, 0.5, 0.75, 1)$.

Plugging of nonlinear continuous functions in Eqs. (7) and (8) into Navier equation in Eq. (6) results in Eq. (9).

$$\left(-\frac{\lambda_2}{r^2}+\frac{\lambda_1(\beta_1+\beta_3)}{r^2}\right)u_r(r)+\frac{(1+\beta_1+\beta_3)}{r}\frac{du_r(r)}{dr}+\frac{d^2u_r(r)}{dr}=-\frac{r(\frac{r}{b})^{-\beta_1+\beta_2}\omega^2\rho_b}{C_o} \tag{9}$$

In Eq. (9), λ_2 stands for the anisotropy/polar degree of the disk material [24].

$$C_o=\frac{C_{11}(r)}{(\frac{r}{b})^{\beta_1}}=-\frac{E_\theta^b \nu_{r\theta}}{\nu_{\theta r}(\nu_{r\theta}\nu_{\theta r}-1)} \tag{10}$$

$$\lambda_1=\frac{C_{12}(r)}{C_{11}(r)}=\nu_{\theta r}=\lambda_2\nu_{r\theta} \tag{11}$$

$$\lambda_2=\frac{C_{22}(r)}{C_{11}(r)}=\frac{E_\theta(r)}{E_r(r)}=\frac{\nu_{\theta r}}{\nu_{r\theta}} \tag{12}$$

In the present study both the homogeneous and particular solutions to the governing equation in Eq. (9) are obtained by using Cauchy-Euler Technique under the considered boundary conditions since Eq. (9) has now constants coefficients. It may be also noted that due to the nature of the chosen grading and profile functions, both λ_1 and λ_2 remain constant along the radial coordinate.

2.1. Analytical Solution under Pressure Loads

Let p_a be the internal pressure, and p_b be the external pressure. If Navier equation in Eq. (9) is solved with $\omega = 0$ under boundary conditions defined at the inner and outer surfaces, $\sigma_r(a) = p_a$ and $\sigma_r(b) = p_b$, the homogeneous solutions are obtained as follows

$$\sigma_r = \frac{r^{\frac{1}{2}(-2-\xi-\beta_1-\beta_3)}}{2}\begin{pmatrix} 2(B_1+B_2r^{\xi})C_{12}(r) \\ +C_{11}\begin{pmatrix} -B_1\xi+B_2r^{\xi}\xi \\ -(B_1+B_2r^{\xi})(\beta_1+\beta_3)\end{pmatrix}\end{pmatrix} \tag{13}$$

$$u_r(r) = r^{\frac{1}{2}(-\xi-\beta_1-\beta_3)}(B_1+B_2r^{\xi}) \tag{14}$$

$$\sigma_\theta = \frac{r^{\frac{1}{2}(-2-\xi-\beta_1-\beta_3)}}{2}\begin{pmatrix} 2(B_1+B_2r^{\xi})C_{22}(r) \\ +C_{12}\begin{pmatrix} -B_1\xi+B_2r^{\xi}\xi \\ -(B_1+B_2r^{\xi})(\beta_1+\beta_3)\end{pmatrix}\end{pmatrix} \tag{15}$$

where

$$\xi = \sqrt{(\beta_1+\beta_3)(\beta_1+\beta_3-4\lambda_1)+4\lambda_2} \tag{16}$$

$$B_1 = \frac{(\frac{a}{b})^{-\beta_1}\begin{pmatrix} 2a^{\xi}p_b(\frac{a}{b})^{\beta_1}b^{\frac{1}{2}(\beta_1+\beta_3+\xi+2)} \\ -2p_ab^{\xi}a^{\frac{1}{2}(\beta_1+\beta_3+\xi+2)}\end{pmatrix}}{C_o(a^{\xi}-b^{\xi})(\beta_1+\beta_3-2\lambda_1+\xi)} \tag{17}$$

$$B_2 = \frac{(\frac{a}{b})^{-\beta_1}\begin{pmatrix} -2p_b(\frac{a}{b})^{\beta_1}b^{\frac{1}{2}(\beta_1+\beta_3+\xi+2)} \\ +2p_aa^{\frac{1}{2}(\beta_1+\beta_3+\xi+2)}\end{pmatrix}}{C_o(a^{\xi}-b^{\xi})(\beta_1+\beta_3-2\lambda_1+\xi)} \tag{18}$$

If the above constants in Eqs. (16), (17) and (18) are plugged into Eq. (13) the radial stress variation is obtained in an explicit form such as

$$\sigma_r = \frac{p_a(\frac{a}{b})^{-\beta_1}a^{\frac{\beta_1+\beta_3+\xi+2}{2}}(\frac{r}{b})^{\beta_1}(b^{\xi}-r^{\xi})r^{\frac{-\beta_1-\beta_3-\xi-2}{2}}}{a^{\xi}-b^{\xi}} + \frac{p_b(a^{\xi}-r^{\xi})b^{\frac{\beta_1+\beta_3+\xi+2}{2}}(\frac{r}{b})^{\beta_1}r^{\frac{-\beta_1-\beta_3-\xi-2}{2}}}{b^{\xi}-a^{\xi}} \tag{19}$$

2.2. Analytical Solution under Centrifugal Forces

The elastic fields due to the centrifugal force with a constant circular velocity is found by solving Eq. (9) in a nonhomogeneous form as follows

$$\sigma_r(r) = \frac{r^{\frac{1}{2}(-2-\xi-\beta_1-\beta_3)}(\frac{r}{b})^{-\beta_1}}{2}\begin{pmatrix} -2r^{\frac{1}{2}(6+\xi+\beta_1+\beta_3)}(\frac{r}{b})^{\beta_2}\Omega\begin{pmatrix} -C_{12}(r)+C_{11}(r) \\ (-3+\beta_1-\beta_2)\end{pmatrix} \\ +(\frac{r}{b})^{\beta_1}\begin{pmatrix}\begin{pmatrix} 2C_{12}(r) \\ (C_1+C_2r^{\xi})\end{pmatrix}+C_{11}(r)\begin{pmatrix} -C_1\xi+C_2r^{\xi}\xi \\ -(C_1+C_2r^{\xi}) \\ (\beta_1+\beta_3)\end{pmatrix}\end{pmatrix}\end{pmatrix} \tag{20}$$

$$u_r(r) = r^{\frac{1}{2}(-\xi-\beta_1-\beta_3)}(C_1+C_2r^{\xi})+r^3(\frac{r}{b})^{-\beta_1+\beta_2}\Omega \tag{21}$$

$$\sigma_\theta(r) = \frac{r^{\frac{1}{2}(-2-\xi-\beta_1-\beta_3)}(\frac{r}{b})^{-\beta_1}}{2}\begin{pmatrix} -2r^{\frac{1}{2}(6+\xi+\beta_1+\beta_3)}(\frac{r}{b})^{\beta_2}\Omega\begin{pmatrix} -C_{22}(r)+C_{12}(r) \\ (-3+\beta_1-\beta_2)\end{pmatrix} \\ +(\frac{r}{b})^{\beta_1}\begin{pmatrix}\begin{pmatrix} 2C_{22}(r) \\ (C_1+C_2r^{\xi})\end{pmatrix}+C_{12}(r)\begin{pmatrix} -C_1\xi+C_2r^{\xi}\xi \\ -(C_1+C_2r^{\xi}) \\ (\beta_1+\beta_3)\end{pmatrix}\end{pmatrix}\end{pmatrix} \tag{22}$$

where

$$\Omega = \frac{\omega^2\rho_b}{C_o\begin{pmatrix} -9-3\beta_3-\beta_2(6+\beta_2+\beta_3) \\ +\beta_1(3+\beta_2+\beta_3-\lambda_1)-\beta_3\lambda_1+\lambda_2\end{pmatrix}} \tag{23}$$

After plugging the boundary conditions given in Table 1, integration constants in solutions (20), (21) and (22) are determined explicitly as shown in Table 2.

Table 1. Boundary conditions for centrifugal loads.

	$r=a$	$r=b$
Free-Free	$\sigma_r(a)=0$	$\sigma_r(b)=0$
Fixed-Free	$u_r(a)=0$	$\sigma_r(b)=0$
Fixed-Guided	$u_r(a)=0$	$u_r(b)=0$

3. Validation of the Results

In this section, four test examples for both uniform and hyperbolic rotating disks are to be studied to verify the analytical solutions developed in the present study. It is worth noting that all these test problems are related to the centrifugal forces. In each sub-section, the existing scope of the test examples has been originally broadened to include pressure loads and hyperbolic profiles.

Dimensionless quantities in the disk subjected to the centrifugal forces are defined as in Eq. (24). Dimensionless quantities used for the pressure loads are explained in the related figure and tables.

$$\overline{\sigma_r}(r)=\frac{\sigma_r(r)}{\rho_o\omega^2b^2},\ \overline{\sigma_\theta}(r)=\frac{\sigma_\theta(r)}{\rho_o\omega^2b^2},\ \overline{u_r}(r)=\frac{E_o u_r(r)}{\rho_o\omega^2b^3} \quad (24)$$

Table 2. Integration constants in solutions (20), (21), and (22).

Free-Free (Rotation)

$$C_1=\frac{2a^{\xi/2}\Omega(\beta_1-\beta_2-\lambda_1-3)b^{\xi/2}(\frac{a}{b})^{-\beta_1}}{(a^\xi-b^\xi)(\beta_1+\beta_3-2\lambda_1+\xi)}\phi_1$$

$$C_2=\frac{2\Omega(\beta_1-\beta_2-\lambda_1-3)b^{\xi/2}(\frac{a}{b})^{-\beta_1}}{(a^\xi-b^\xi)(\beta_1+\beta_3-2\lambda_1-\xi)}\phi_2$$

$$\phi_1=a^{\frac{\beta_1+\beta_3+6}{2}}b^{\frac{\xi}{2}}(\frac{a}{b})^{\beta_2}-a^{\frac{\xi}{2}}b^{\frac{\beta_1+\beta_3+6}{2}}(\frac{a}{b})^{\beta_1}$$

$$\phi_2=b^{\frac{\beta_1+\beta_3+\xi+6}{2}}(\frac{a}{b})^{\beta_1}-a^{\frac{\beta_1+\beta_3+\xi+6}{2}}(\frac{a}{b})^{\beta_2}$$

Fixed-Free (Rotation)

$$C_1=\frac{(\frac{a}{b})^{-\beta_1}}{(a^\xi-b^\xi)(\beta_1+\beta_3-2\lambda_1)+\xi(a^\xi+b^\xi)}\phi_3$$

$$C_2=\frac{(\frac{a}{b})^{-\beta_1}}{(a^\xi-b^\xi)(\beta_1+\beta_3-2\lambda_1)+\xi(a^\xi+b^\xi)}\phi_4$$

$$\phi_3=\begin{pmatrix}-b^\xi\Omega(\frac{a}{b})^{\beta_2}a^{\frac{\beta_1+\beta_3+\xi+6}{2}}(-\beta_1-\beta_3+2\lambda_1+\xi)\\-2a^\xi\Omega(\frac{a}{b})^{\beta_1}b^{\frac{\beta_1+\beta_3+\xi+6}{2}}(\beta_1-\beta_2-\lambda_1-3)\end{pmatrix}$$

$$\phi_4=\begin{pmatrix}2\Omega(\frac{a}{b})^{\beta_1}b^{\frac{\beta_1+\beta_3+\xi+6}{2}}(\beta_1-\beta_2-\lambda_1-3)\\-\Omega(\frac{a}{b})^{\beta_2}a^{\frac{\beta_1+\beta_3+\xi+6}{2}}(\beta_1+\beta_3-2\lambda_1+\xi)\end{pmatrix}$$

Fixed-Guided (Rotation)

$$C_1=\frac{\Omega\left(b^\xi(\frac{a}{b})^{\beta_2-\beta_1}a^{\frac{\beta_1+\beta_3+\xi+6}{2}}-a^\xi b^{\frac{\beta_1+\beta_3+\xi+6}{2}}\right)}{a^\xi-b^\xi}$$

$$C_2=\frac{\Omega\left(-(\frac{a}{b})^{\beta_2-\beta_1}a^{\frac{\beta_1+\beta_3+\xi+6}{2}}+b^{\frac{\beta_1+\beta_3+\xi+6}{2}}\right)}{a^\xi-b^\xi}$$

3.1. Test Example I: Polar Orthotropic Uniform Disk

Yıldırım [24] studied analytically and numerically the elastic behaviour of uniform ordinary polar orthotropic rotating disks under various boundary conditions. The complementary functions method (CFM) was employed in the numerical study. By using the same gradation rule in Eqs. (7) and (8), anisotropy effects were investigated by either physically anisotropic (Table 3) or hypothetically anisotropic materials in a detailed manner in that study. The necessary data for this test example is: $a=2cm$, $b=5cm$, $\rho_o=\rho_b$, $E_o=E_\theta^b$, and $\beta_1=\beta_2=\beta_3=0$. Table 4 shows the comparison of some numerical results under rotation. The perfect conformity of the present analytical and the literature numerical results for the rotating uniform disks made of five different physical orthotropic materials is observed from Table 4 ($p_b=0$). The additional results for the extension of the test example to the uniform polar orthotropic stress-free disks under internal pressure are also included in the same table together with Table 5.

Table 3. Material properties considered in Test Example I.

Material	E_r(GPa)	E_θ(GPa)	ρ ($\frac{kg}{m^3}$)	$\nu_{r\theta}$
MAT-1	2.2	2.2	1220	0.3
MAT-2	28.6	8.27	1800	0.26
MAT-3	181.	10.3	1600	0.28
MAT-4	21.8	26.95	2030	0.15
MAT-5	12.0	20.0	1600	0.21

As seen from Tables 4-5, MAT-3 offers the smallest maximum hoop stress under the internal pressure and under the rotation with fixed-free and fixed-guided boundaries, while MAT-4 seems to have the best hoop stress under stress-free rotation.

Effects of the disk profile on the elastic fields in the disk made of MAT-3 under internal pressure is illustrated in Figure 5.

Table 4. Comparison of the present results with the literature for the test example I.

	$\overline{\sigma_\theta}(a)$ (Due to Rotation)		
	Free-Free	**Fixed-Free**	**Fixed-Guided**
Numerical-CFM [24]			
MAT-1	0.853000	0.1522351	0.063000
MAT-2	0.849296	0.0509403	0.016852
MAT-3	0.851131	0.0120589	0.003651
MAT-4	0.815113	0.0926972	0.038137
MAT-5	0.823848	0.1510878	0.069357
Present (Analytical)			
MAT-1	0.853	0.152235	0.063
MAT-2	0.849296	0.0509403	0.016852
MAT-3	0.851131	0.0120589	0.003651
MAT-4	0.815113	0.0926972	0.038137
MAT-5	0.823848	0.151088	0.069357
Expanded present results to the inner pressure			
	$u_r(a)/b$	$\sigma_r(0.7)/p_a$	$\sigma_\theta(a)/p_a$
MAT-1	0.305628	-0.198251	1.38095
MAT-2	0.060627	-0.214995	1.17828
MAT-3	0.043674	-0.220939	1.10868
MAT-4	0.024202	-0.193125	1.44515
MAT-5	0.038169	-0.184289	1.55847

Table 5. Broadening of example I to the convergent hyperbolic RR-disks under internal pressure ($\beta_3 = -0.75$).

r/b	u_r/b	σ_r/p_a	σ_θ/p_a
MAT-1 (Polycarbonate)			
0.4	0.391764	-1.	1.8547
0.6	0.297652	-0.381632	0.976902
0.8	0.253943	-0.132827	0.658495
1.	0.232702	0.	0.511944
MAT-2 (GFRP (E-Glass/Epoxy))			
0.4	0.0815545	-1.	1.61096
0.6	0.0746446	-0.413212	0.997786
0.8	0.0712435	-0.148253	0.725333
1.	0.0695977	0.	0.575573
MAT-3 (CFRP (T300/N5208))			
0.4	0.0600208	-1.	1.5296
0.6	0.0588995	-0.424107	1.00435
0.8	0.0583287	-0.15364	0.748534
1.	0.0580444	0.	0.597857
MAT-4 (A Glass Fiber/Epoxy Prepreg)			
0.4	0.030868	-1.	1.89431
0.6	0.023225	-0.376652	0.973338
0.8	0.019954	-0.130422	0.648017
1.	0.018629	0.	0.502052
MAT-5 (An injection molded Nylon 6 composite containing 40wt% short glass fiber)			
0.4	0.047713	-1.	2.03562
0.6	0.032579	-0.35924	0.960242
0.8	0.026170	-0.122076	0.61152
1.	0.023390	0.	0.467783

Figure 5 implies that the maximum hoop stresses are at the inner surface for all disk profiles under pressure. The distribution of the radial displacement is almost uniform for all profile parameters. The divergent disk profiles seem to be better than the convergent ones for the radial displacement and hoop stresses. That is the thicker thickness at the outer surface is preferable for the pressure loads acting on the inner surface of an orthotropic hyperbolic disk.

Broadening of example I to the free-free and fixed-free hyperbolic rotating RR disks made of MAT-3 is shown in Figure 6. This figure reveals that convergent disk profiles should be preferred under rotation for both free-free and fixed-free boundary conditions. Apart from this, fixed-free boundary condition offers the smallest radial displacement and hoop stresses for all disk profiles. The smallest maximum radial stresses are observed in free-free hyperbolic disks subjected to the centrifugal forces.

Table 6. Broadening of example II to the FG-isotropic hyperbolic disks under internal and external pressures.

r/b	$\beta_3 = 0.5$	$\beta_3 = 0$	$\beta_3 = -0.5$
u_r/b			
0.2	5.60162	6.22324	7.00161
0.4	0.136982	0.241776	0.412894
0.6	0.017527	0.061365	0.14131
0.8	0.005488	0.038893	0.100693
1.	0.003169	0.033547	0.089753
σ_r/p_a			
0.2	-1.	-1.	-1.
0.4	-0.38420	-0.53298	-0.73631
0.6	-0.21858	-0.35445	-0.57518
0.8	-0.14416	-0.23119	-0.38817
1.	-0.1	-0.1	-0.1
σ_θ/p_a			
0.2	-0.12075	-0.10086	-0.07595
0.4	-0.04513	-0.03611	-0.00949
0.6	-0.02015	0.052722	0.193724
0.8	0.001711	0.249255	0.708424
1.	0.033380	0.640938	1.76506

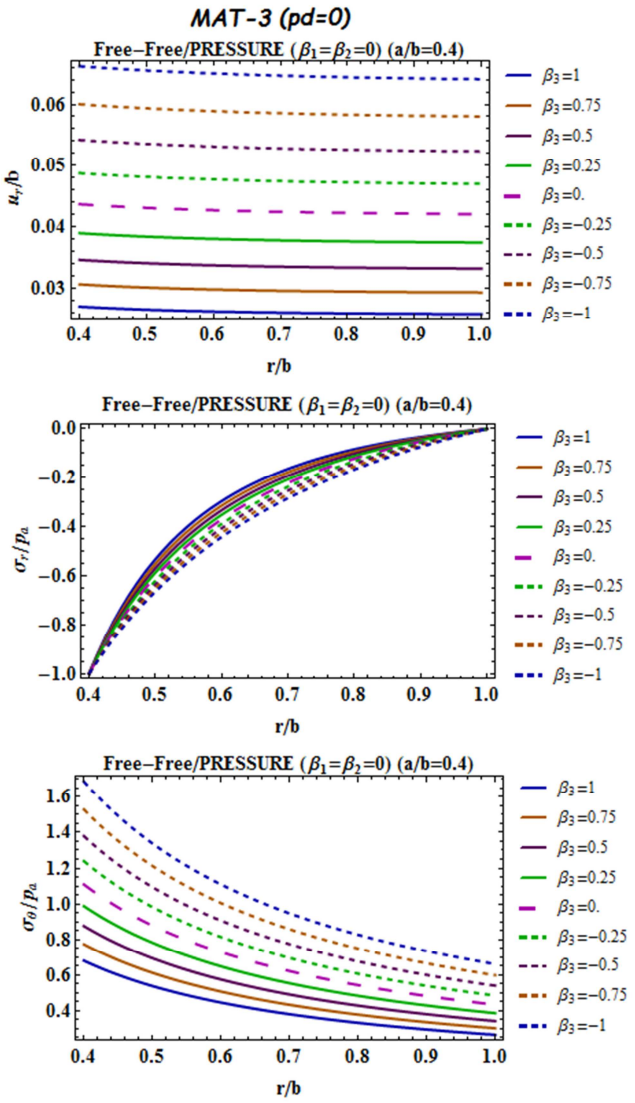

Figure 5. Broadening of example I to the hyperbolic RR disks made of CFRP and subjected to the internal pressure.

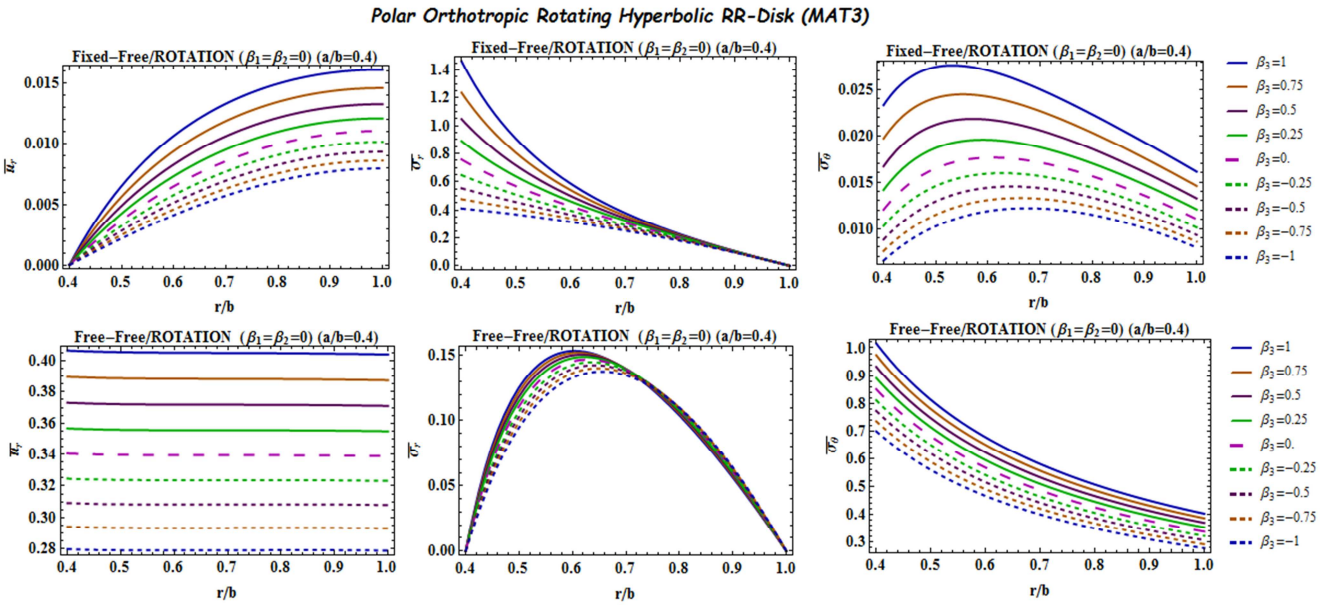

Figure 6. Broadening of example I to the hyperbolic rotating RR disks made of CFRP (T300/N5208) material.

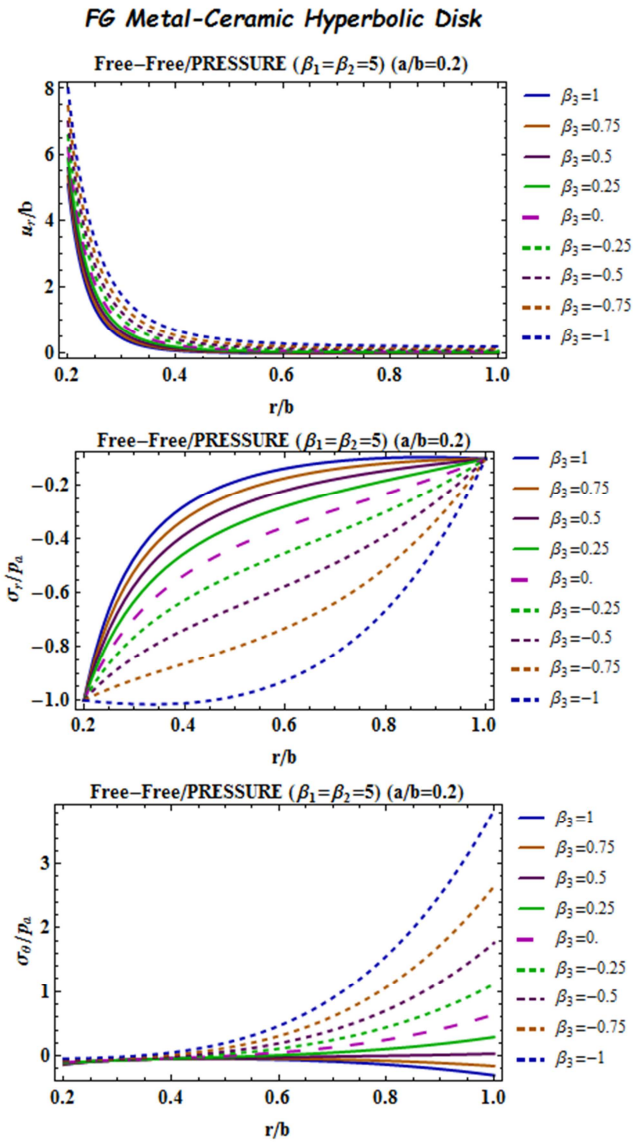

Figure 7. Broadening of example II to the hyperbolic pressurized FG metal-ceramic disks for $\beta_1 = \beta_2 = 5$.

3.2. Test Example II: FG-Isotropic Hyperbolic Disk (Metal-Ceramic Composition)

Here Yıldırım's [49] study for a power-law graded isotropic and nonhomogeneous hyperbolic rotating disk is to be considered. The material grading rule is the same with the present study and $a/b = 0.2$. In this section $\lambda_1 = \nu$, $\lambda_2 = 1$, $E(r) = E_r(r) = E_\theta(r)$ and $\nu = \nu_{r\theta} = \nu_{\theta r}$ for isotropic materials. Due to perfect overlapping the present and Yıldırım's [49] results under rotation, they are not to be repeated here. Instead of this, this example [49] is to be extended to the pressure loads ($p_a / p_b = 10$) for $\beta_1 = \beta_2 = 5$ as seen in Figure 7 and Table 6.

For $\beta_1 = \beta_2 = 5$, from Figure 7 and Table 6, the maximum hoop stress due to internal and external pressures is either at the outer surface or at the inner surface. If divergent profiles are considered, it is at the inner surface. However it was at the inner surface in the first test example of orthotropic convergent/divergent hyperbolic disks when $\beta_1 = \beta_2 = 0$ (Figure 5). The distribution of the radial displacement is not almost uniform anymore as in the previous example. Divergent profiles seems to be still better to get smaller radial displacements and circumferential stresses.

3.3. Test Example III: FG-Polar Orthotropic Uniform Disk

Peng and Li's [55] benchmark example is now considered to validate the present results. Material and geometric properties are: $a/b = 0.4$, $\rho_b = 1600\ kg/m^3$, $E_r^b = 12\ GPa$, $E_\theta^b = 20\ GPa$, $\nu_{\theta r} = 0.35$. Peng and Li [55] used $\rho_o = \rho_b$, and $E_o = E_\theta^b$ in their results for RR-disks in the case of $\beta = \beta_1 = \beta_2 = -1, 0, 1, 2$ and $\beta_3 = 0$.

For uniform disks subjected to the centrifugal forces, the present results are validated by Figure 8 and Table 7. An excellent accordance between the analytical solutions is observed in Table 7. Table 7 also comprises the spreading of the third example for the remaining two boundary conditions and CR-disks for $\beta = 2$. As observed from Table 7, free-free CR-disks have higher elastic fields than RR-disks.

As to fixed-free and fixed-fixed CR-disks, from Table 7, they have smaller radial displacements, higher radial stresses, and smaller hoop stresses than RR-disks.

As in the previous examples, this test example is also originally studied under internal pressure (Table 8, Figure 9). It is observed from both Table 8 and Figure 9 that negative inhomogeneity indexes offer smaller radial displacements and higher hoop stresses than the positive ones. Maximum radial displacements are at the inner surface for both CR and RR disks.

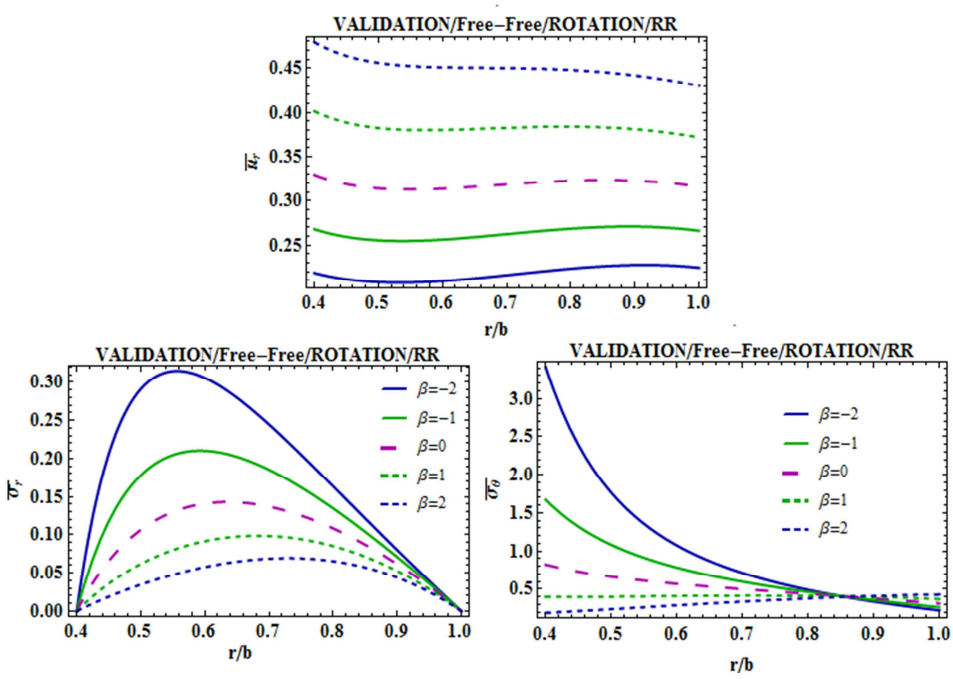

Figure 8. Validation the present formulas (Example III).

Table 7. Comparison of the results for the third example under rotation ($\beta = \beta_1 = \beta_2 = 2$).

r/b	$\overline{u_r}$	$\overline{\sigma_r}$	$\overline{\sigma_\theta}$
Free-Free (RR) – Present Analytical			
0.4	0.479373	0.	0.191749
0.6	0.451231	0.0576996	0.290933
0.8	0.448301	0.065374	0.381522
1.	0.43026	0.	0.43026
Free-Free (RR) – Analytical [55]			
0.4	0.4794	0.	0.1917
0.6	0.4512	0.0577	0.2909
0.8	0.4483	0.0654	0.3815
1.	0.4303	0.	0.4303
Free-Free (CR) – Present Analytical			
0.4	0.492324	0.	0.19693
0.6	0.465472	0.0590431	0.291682
0.8	0.453201	0.0656418	0.376346
1.	0.438184	0.	0.438184
Fixed-Free (RR) – Present Analytical			
0.4	0.	0.194701	0.0681452
0.6	0.204037	0.148604	0.174434
0.8	0.263855	0.102479	0.246952
1.	0.266661	0.	0.266661
Fixed-Free (CR) – Present Analytical			
0.4	0.	0.3077	0.0646171
0.6	0.115702	0.212841	0.114118
0.8	0.148613	0.130124	0.146217
1.	0.152021	0.	0.152021
Fixed-Fixed (RR) – Present Analytical			
0.4	0.	0.0495967	0.0173589
0.6	0.0443272	0.01974	0.0335053
0.8	0.0376673	-0.0405807	0.0159306
1.	0.	-0.170072	-0.059525
Fixed-Fixed (CR) – Present Analytical			
0.4	0.	0.0533737	0.0112085
0.6	0.0170416	0.0175686	0.0139143
0.8	0.0142096	-0.0469636	0.0015053
1.	0.	-0.175021	-0.0367543

After $\beta \geq 2$, the location the maximum hoop stress is shifted from the inner surface towards the outer surface. While $\beta = 2$ seems to be an appropriate inhomogeneity index for the hoop stresses due to almost uniform radial distribution for

RR-disk, $\beta = 1$ presents the best almost uniform hoop stress distribution for CR- disk.

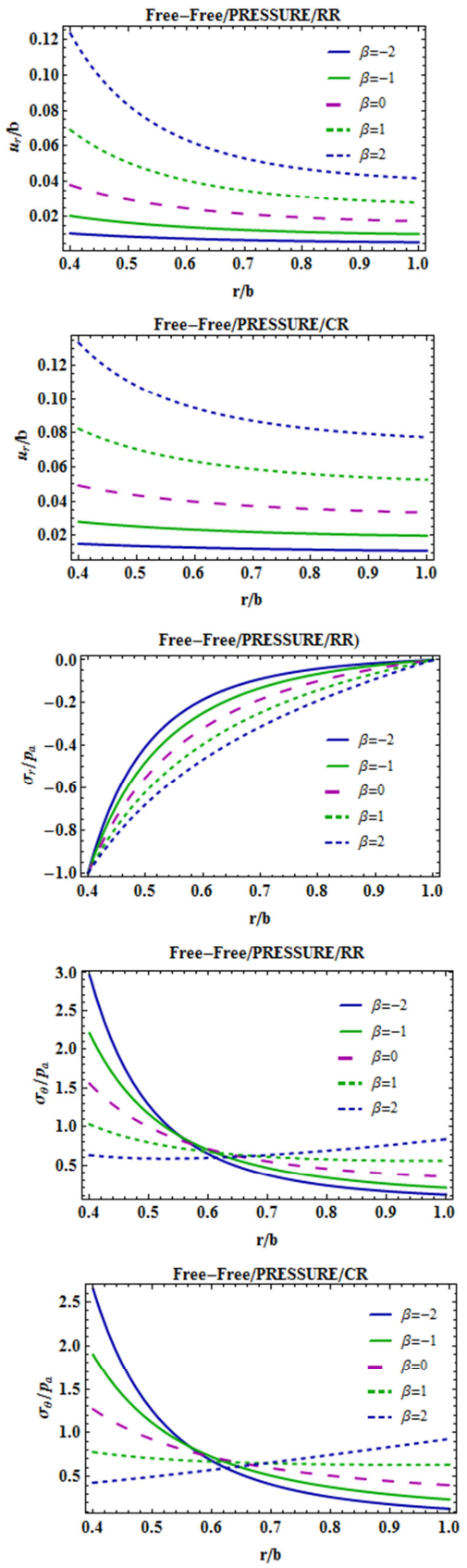

Figure 9. The third example with the inner pressure.

Table 8. The present results for a uniform disk subjected to an internal pressure (Example III).

r/b	u_r/b	σ_r/p_a	σ_θ/p_a
	$\beta=-1$		
Free-Free (RR)			
0.4	0.0204737	-1.	2.20921
0.6	0.0141824	-0.247836	0.70117
0.8	0.0114452	-0.0650443	0.334898
1.	0.0102351	0.	0.204702
Free-Free (CR)			
0.4	0.0280987	-1.	1.8974
0.6	0.0234702	-0.275001	0.72459
0.8	0.0211359	-0.0751989	0.380506
1.	0.019919	0.	0.239028
	$\beta=0$		
Free-Free (RR)			
0.4	0.0381694	-1.	1.55847
0.6	0.0247498	-0.319332	0.713229
0.8	0.0195726	-0.0987575	0.454749
1.	0.0174604	0.	0.349209
Free-Free (CR)			
0.4	0.0492914	-1.	1.26874
0.6	0.0398387	-0.351199	0.723023
0.8	0.0355737	-0.112671	0.509944
1.	0.0334947	0.	0.401936
	$\beta=1$		
Free-Free (RR)			
0.4	0.0691275	-1.	1.03255
0.6	0.0407784	-0.394493	0.677495
0.8	0.0314331	-0.141357	0.579188
1.	0.027965	0.	0.5593
Free-Free (CR)			
0.4	0.0825141	-1.	0.78017
0.6	0.063403	-0.428544	0.670841
0.8	0.0560008	-0.158533	0.638718
1.	0.0526739	0.	0.632087

3.4. Test Example IV: FG- Polar Orthotropic Uniform and Hyperbolic Disks

In this section Essa and Argeso's [57] test examples are considered for uniform and hyperbolic rotating RR disks made of FG polar orthotropic materials. Essa and Argeso [57] have used a simple power law variation as follows (Figure 10): $E(r) = E_r^a (r/a)^{\beta_1}$, $\rho(r) = \rho_a (r/a)^{\beta_2}$, $h(r) = h_o (r/a)^{\beta_3}$. After modifying their data for the present study, the common properties of both examples are to be: $a/b = 0.4$, $\rho_b = 2.5^{-0.8}$, $\beta_1 = -1$, $\beta_2 = -0.8$, $E_r^b = 0.3$, $E_\theta^b = 0.4$, $\nu_{r\theta} = 0.25$.

Dimensional results are presented in Figure 11 and Table 9. Again, a perfect overlapping is observed between the solutions.

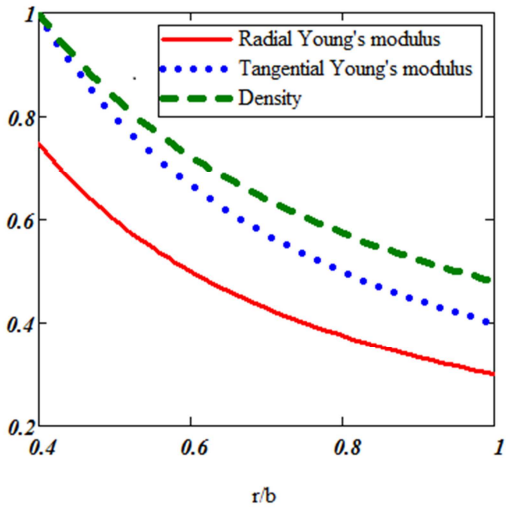

Figure 10. Material property variation for the test example IV.

Table 9. Validation the present formulas for FG polar orthotropic uniform and hyperbolic rotating RR-disks with the literature.

Present and [55]* and [57]			
UNIFORM ($\beta_3 = 0$, $\omega = 1.14613$)			
r/b	u_r	σ_r	σ_θ
0.4	0.399997	0.	0.999993
0.5	0.380673	0.111664	0.646299
0.6	0.378991	0.132946	0.465416
0.7	0.384672	0.118134	0.353396
0.8	0.390988	0.086431	0.273178
0.9	0.392792	0.045812	0.209242
1.	0.385717	0.	0.154287
Present and [57]			
HYPERBOLIC ($\beta_3 = -0.756471$, $\omega = 2.38140$)			
r/b	u_r	σ_r	σ_θ
0.4	0.	1.20829	0.402764
0.5	0.147699	1.0281	0.579018
0.6	0.292261	0.854158	0.609453
0.7	0.424721	0.66711	0.569081
0.8	0.532603	0.462423	0.487018
0.9	0.601218	0.239753	0.376816
1.	0.614277	0	0.245711

*computed and presented by Essa and Argeso [57]

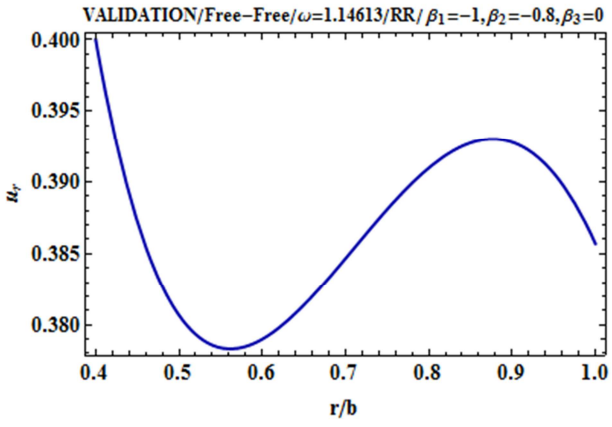

Figure 11. Validation of the radial displacement for example IV.

4. Results and Discussion

Effects of the variation of the profile parameter on the elastic fields i) in FG polar orthotropic hyperbolic disks, ii) in only polar orthotropic hyperbolic disks are studied in the first two sub-sections below in a detailed manner. Finally, effects of the variation of the gradation parameter on the elastic fields in FG polar orthotropic hyperbolic disks is also investigated. Results observed from the fresh examples are discussed in each related sub-sections.

4.1. Effects of the Variation of the Profile Parameter on the Elastic Fields in FG Polar Orthotropic Hyperbolic Disks

In this section effects of the variation of the disk profile parameter on the elastic fields are originally investigated for FG polar orthotropic hyperbolic RR and CR disks having either convergent ($\beta_3 < 0$) or divergent ($\beta_3 > 0$) profiles under both separate centrifugal and pressure loads and different boundary conditions for $\beta = \beta_1 = \beta_2 = 1.5$ and $\beta = -1.5$. Results are presented in Figures 12-13 and Tables 10-12. From those figures and tables, the followings may be observed:

a) For both positive and negative inhomogeneity indexes, all hyperbolic profiles having CR-alignment have smaller radial displacements under fixed-free and fixed-fixed boundary conditions. This is true for the free-free CR-disks subjected to centrifugal forces having negative inhomogeneity indexes.

b) For free-free, fixed-free and fixed-fixed surfaces and under rotation, convergent profiles offer much smaller radial displacements than the divergent ones for all inhomogeneity indexes. This situation is reversed if the disk is subjected to the pressure loads.

c) For fixed-fixed/rotation, the hoop stresses are all in tension-compression. For free-free/pressure, this situation is observed in divergent profiles with $\beta = 1.5$ (Figure 13).

d) The maximum hoop stress is at the outer surface of free-free/rotation disks for positive inhomogeneity indexes while it is at the inner surface for negative inhomogeneity indexes.

e) The maximum hoop stress is at the outer surface of fixed-free/rotation disks for positive inhomogeneity indexes while it is at the vicinity of the inner surface for negative inhomogeneity indexes (Figure 13).

f) If the circumferential stresses in free-free hyperbolic disks are considered (Figure 13), divergent profiles seem to be more proper under pressure loads while convergent profiles exhibit better response to the centrifugal forces.

Apart from those, CR-disks seem to be more appropriate for pressure loads while RR-disks are proper for centrifugal loads.

g) CR-disks subjected to rotation are preferable for both fixed-fixed and fixed-free boundary conditions under all inhomogeneity indexes.

h) Divergent disk profiles are better with positive inhomogeneity indexes while convergent ones are well with negative inhomogeneity indexes for the hoop stresses in fixed-fixed hyperbolic disks.

i) For convergent fixed-free disks subjected to rotation with constant circular speed, both the radial and hoop stresses are much smaller than the divergent ones for all inhomogeneity indexes (Figure 13).

j) Contrary to the hoop stress variations in fixed-free and fixed-fixed hyperbolic disks, CR-alignment offer much higher radial stresses for all inhomogeneity indexes.

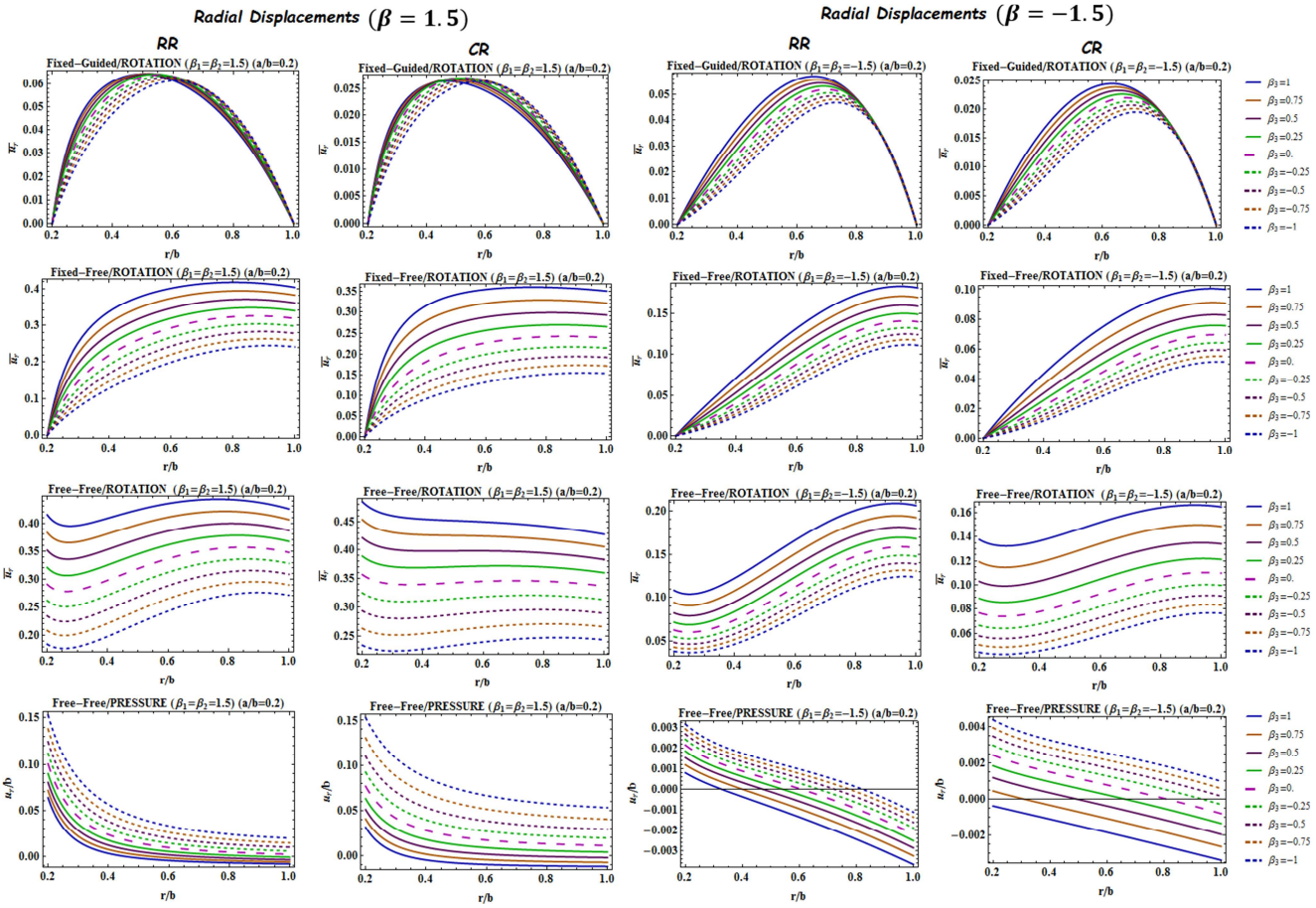

Figure 12. Variation of the radial displacements with profile parameters in RR and CR disks for $\beta = 1.5, -1.5$.

4.2. Effects of the Variation of the Profile Parameter on the Elastic Fields in Polar Orthotropic Hyperbolic Disks

The formulas developed in the present study may be directly used for the hyperbolic disks made of a single orthotropic material by just taking $\beta_1 = \beta_2 = 0$. Results are presented in Figures 14-15 and Tables 13-14 for hyperbolic disks subjected to the either internal/external pressures or centrifugal forces.

Figure 14 implies that divergent profiles are preferable to convergent ones for the disks under pressure. From Table 13 it is revealed that CR-alignments are better than RR-ones under pressure.

Table 14 indicates that RR-convergent disks are the best for the rotation under stress-free boundary conditions. However, from Figure 15 and Table 14, divergent profiles of free-free RR-disk are the best for pressure loads. Table 14 implies that RR-convergent fixed-free polar orthotropic hyperbolic disks are superior to the other types under rotation.

From Figure 15, again, RR-convergent hyperbolic disks are preferable to the RR-divergent ones under fixed-guided boundary conditions.

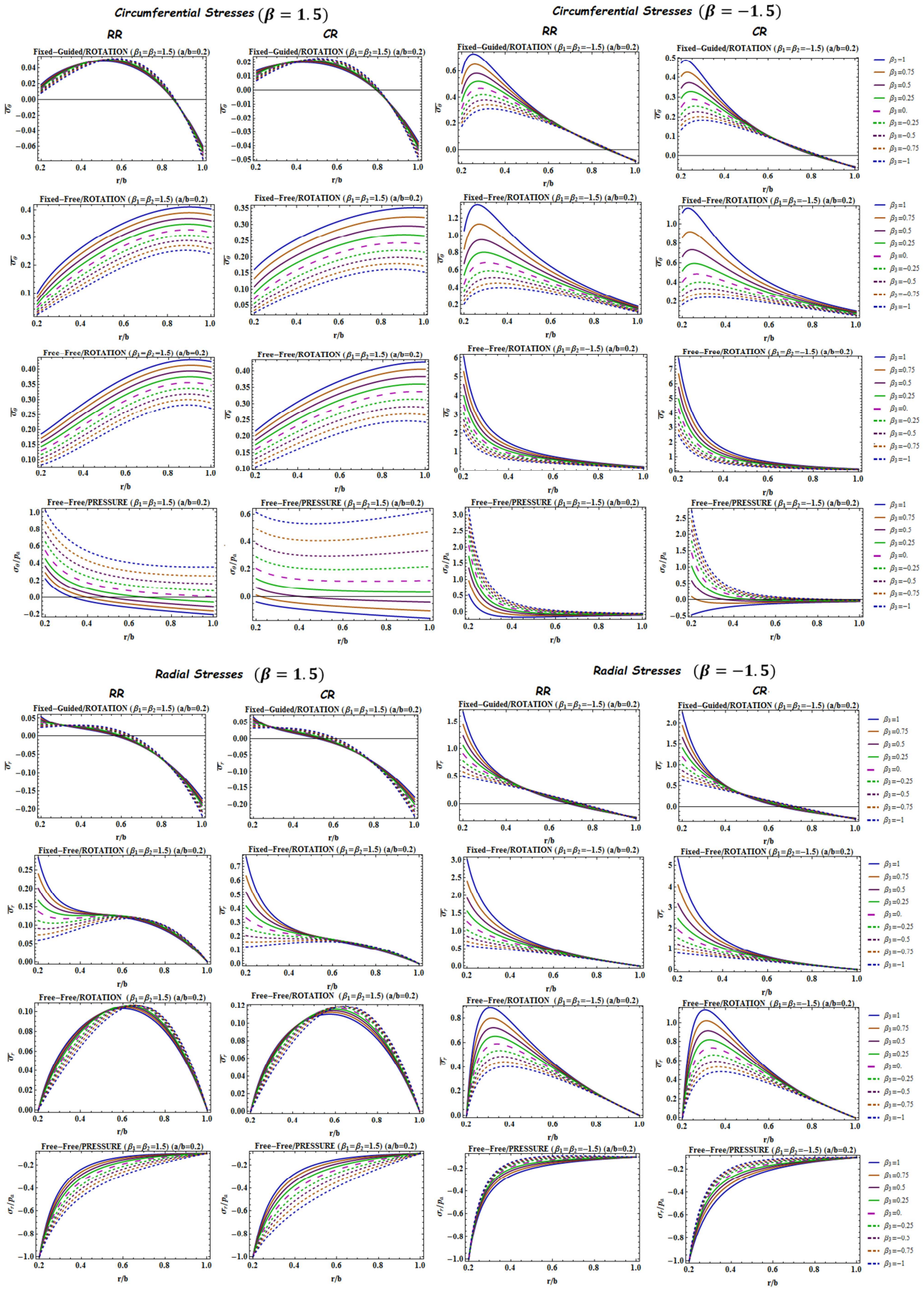

Figure 13. Variation of the stresses with profile parameters in RR and CR disks for $\beta = 1.5, -1.5$.

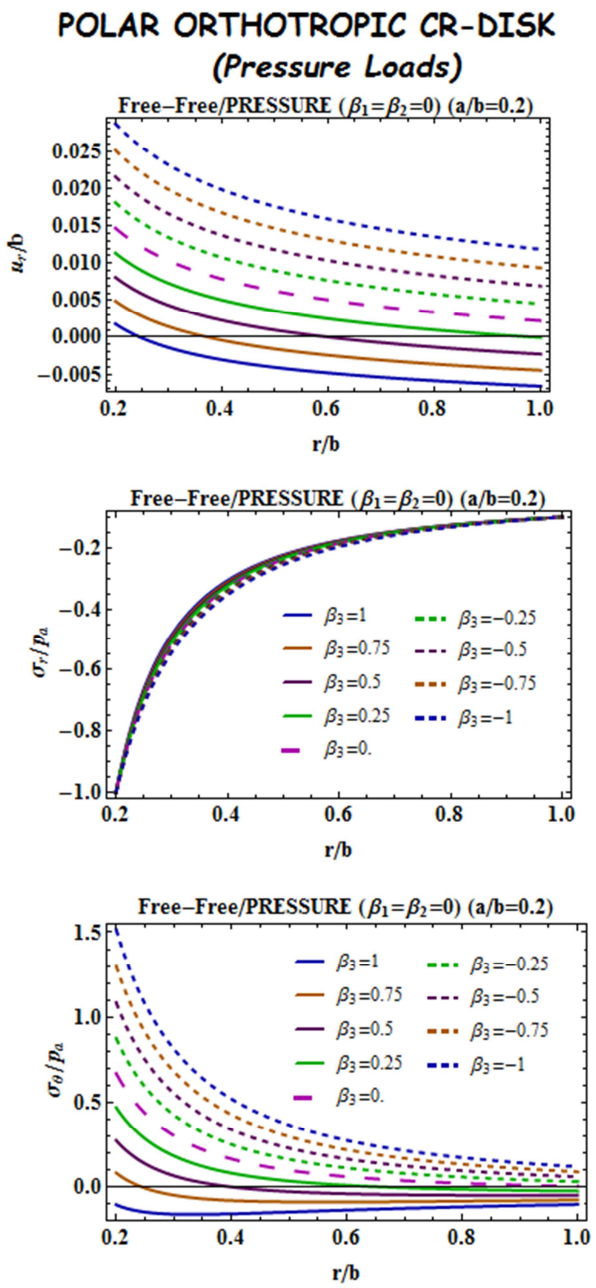

Figure 14. Variation of the elastic fields in a CR-hyperbolic disk made of a single polar orthotropic material under pressure.

4.3. Effects of the Variation of the Gradation Parameter on the Elastic Fields in FG Polar Orthotropic Hyperbolic Disks

As a final example, variation of the equivalent stress, in Eq. (25), with the inhomogeneity index is aimed to be studied under only centrifugal force effects. Results are presented in Figures 16-17. Figure 16 shows the variation of the elastic fields with the gradation parameter in convergent RR hyperbolic rotating disks under fixed-free and free-free boundary conditions.

Variation of the equivalent stresses with the gradation parameter for convergent RR and CR hyperbolic rotating disks under three boundary conditions is illustrated in Figure 17.

$$\sigma_{eq}=\sqrt{\sigma_r^2-\sigma_r\sigma_\theta+\sigma_\theta^2} \tag{25}$$

Figure 17 indicates that positive inhomogeneity indexes are preferable for both CR and RR convergent hyperbolic disks under rotation. CR disks exhibit higher equivalent stresses than RR-ones. It seems possible to achieve the best inhomogeneity index for a given geometry, loading and boundary conditions in the material tailoring. For instance, from Figure 17, $\beta=1$ is to be a good choice to get almost uniform stress distributed along the radial coordinate under free-free condition.

5. Conclusions

A unified formulation is carried out by presuming a state of axisymmetric plane stress and small deformations for the elastic analysis of convergent/divergent hyperbolic thin disks subjected to both internal/external pressure and centrifugal forces under free-free, fixed-free, and fixed-fixed boundary conditions. The disk material is assumed to be functionally graded polar orthotropic material whose fibers aligned totally either in the radial or circumferential directions. A polar orthotropic material without FG, a functionally graded isotropic material which is composed of metal and ceramic pairs, and finally an isotropic and homogeneous conventional material may all be studied by the same closed-form formulas developed and presented in this study. It is also possible to consider concentric disk assembles via these formulas.

Comprehensive investigations conducted in the present study give very useful clues to the engineers:

a) For both positive and negative inhomogeneity indexes, all hyperbolic FG polar orthotropic fixed-free and fixed-fixed CR-disks have smaller radial displacements under rotation. This is true for the free-free CR-disks subjected to centrifugal forces having negative inhomogeneity indexes.

b) For all boundary conditions and inhomogeneity indexes, and under centrifugal forces, convergent FG polar orthotropic disks offer much smaller radial displacements than the divergent ones. This situation is reversed if the disk is subjected to the pressure loads.

c) The maximum hoop stress in FG polar orthotropic traction-free disks under rotation is at the outer surface for positive inhomogeneity indexes while it is at the inner surface for negative inhomogeneity indexes.

d) The maximum hoop stress is at the outer surface of fixed-

free/rotation disks for positive inhomogeneity indexes while it is at the vicinity of the inner surface for negative inhomogeneity indexes.

e) For free-free boundary conditions, CR-disks made of a FG polar orthotropic material seem to be appropriate for pressure loads while RR-disks are proper for centrifugal loads.

f) Divergent profiles of FG polar orthotropic disks seem to have more proper circumferential stress under pressure loads while convergent profiles exhibit better circumferential stress response to the centrifugal forces.

g) CR-disks made of a FG polar orthotropic material and subjected to rotation are preferable for both fixed-fixed and fixed-free boundary conditions under all inhomogeneity indexes.

h) For convergent fixed-free FG polar orthotropic disks under rotation, both the radial and hoop stresses are smaller than the divergent ones for all inhomogeneity indexes.

i) Contrary to the hoop stress variations in fixed-free and fixed-fixed hyperbolic FG polar orthotropic disks under rotation, CR-alignment offer much higher radial stresses for all inhomogeneity indexes.

j) Divergent profiles are preferable to convergent ones for the polar orthotropic disks under pressure. CR-alignments are better than RR-ones under pressure.

k) RR-convergent disks are the best for the rotation of polar orthotropic disks under stress-free boundary conditions. However, divergent profiles of free-free RR-disk are the best for pressure loads.

l) RR-convergent fixed-free polar orthotropic hyperbolic disks are superior to the other types under rotation.

m) Positive inhomogeneity indexes are preferable for both CR and RR convergent FG polar orthotropic hyperbolic disks under rotation. CR disks exhibit higher equivalent stresses than RR-ones.

Table 10. The present results for a hyperbolic disk subjected to centrifugal forces for $\beta_1 = \beta_2 = 1.5$.

r/b	$\overline{u_r}$	$\overline{\sigma_r}$	$\overline{\sigma_\theta}$	$\overline{u_r}$	$\overline{\sigma_r}$	$\overline{\sigma_\theta}$
	$\beta_3 = 0.75$ **(Divergent)**			$\beta_3 = -0.75$ **(Convergent)**		
Free-Free (RR)						
0.2	0.38339	0.	0.171457	0.208435	0.	0.0932149
0.4	0.381144	0.0825583	0.269952	0.22116	0.0680363	0.163687
0.6	0.410732	0.104484	0.354722	0.26511	0.10443	0.241904
0.8	0.421172	0.0820887	0.405438	0.292281	0.0915753	0.293475
1.	0.406552	0.	0.406552	0.28982	0.	0.28982
r/b	$\overline{u_r}$	$\overline{\sigma_r}$	$\overline{\sigma_\theta}$	$\overline{u_r}$	$\overline{\sigma_r}$	$\overline{\sigma_\theta}$
	$\beta_3 = 0.75$ **(Divergent)**			$\beta_3 = -0.75$ **(Convergent)**		
Free-Free (CR)						
0.2	0.453085	0.	0.202626	0.263237	0.	0.117723
0.4	0.426497	0.0936299	0.289403	0.254251	0.082508	0.178129
0.6	0.424368	0.112129	0.352261	0.265233	0.118388	0.23031
0.8	0.418752	0.0845734	0.392304	0.271033	0.0984527	0.263094
1.	0.405956	0.	0.405956	0.266212	0.	0.266212
Fixed-Free (RR)						
0.2	0.	0.23946	0.0838109	0.	0.0737319	0.0258062
0.4	0.305519	0.135453	0.240636	0.147407	0.099095	0.127912
0.6	0.373315	0.123367	0.332347	0.220417	0.120246	0.21282
0.8	0.393515	0.0884893	0.382942	0.257589	0.0983641	0.264822
1.	0.382041	0.	0.382041	0.258934	0.	0.258934
Fixed-Free (CR)						
0.2	0.	0.634464	0.133237	0.	0.158741	0.0333356
0.4	0.27787	0.257969	0.229914	0.108308	0.166503	0.103465
0.6	0.321442	0.174695	0.285674	0.151422	0.16501	0.151943
0.8	0.329495	0.106329	0.317039	0.170208	0.119138	0.177257
1.	0.322124	0.	0.322124	0.171352	0.	0.171352
Fixed-Fixed (RR)						
0.2	0.	0.0501133	0.0175396	0.	0.0267574	0.00936507
0.4	0.06017	0.0216759	0.0456414	0.0495861	0.0286552	0.0413903
0.6	0.0621763	-0.0033169	0.0470006	0.0621441	0.00979676	0.0515655
0.8	0.0423046	-0.0622319	0.0160572	0.0471936	-0.0600303	0.0212006
1.	0.	-0.177149	-0.0620021	0.	-0.211994	-0.0741979
Fixed-Fixed (CR)						
0.2	0.	0.0620087	0.0130218	0.	0.0355593	0.00746746
0.4	0.0256375	0.0180439	0.0200038	0.0225922	0.0290023	0.020379
0.6	0.0250689	-0.0136436	0.0165531	0.0264682	-0.00029059	0.0204412
0.8	0.016375	-0.0741971	-0.00093517	0.0190623	-0.0772639	0.000824389
1.	0.	-0.18506	-0.0388627	0.	-0.228594	-0.0480048

Table 11. The present results for a hyperbolic disk subjected to centrifugal forces for $\beta_1 = \beta_2 = -1.5$.

r/b	$\overline{u_r}$	$\overline{\sigma_r}$	$\overline{\sigma_\theta}$	$\overline{u_r}$	$\overline{\sigma_r}$	$\overline{\sigma_\theta}$
	$\beta_3 = 0.75$ **(Divergent)**			$\beta_3 = -0.75$ **(Convergent)**		
Free-Free (RR)						
0.2	0.094261	0.	5.26935	0.0429442	0.	2.40065
0.4	0.107816	0.722143	1.3182	0.051807	0.438215	0.665338
0.6	0.150526	0.420729	0.687054	0.0848594	0.329861	0.419765
0.8	0.185629	0.182254	0.388069	0.119291	0.17113	0.268289
1.	0.192386	0.	0.192386	0.130792	0.	0.130792
Free-Free (CR)						
0.2	0.11909	0.	6.65731	0.0505046	0.	2.82329
0.4	0.118871	0.895013	1.36265	0.0518455	0.528195	0.623264
0.6	0.134381	0.488507	0.58449	0.0649005	0.378364	0.312196
0.8	0.147074	0.200496	0.299031	0.0786172	0.187584	0.176731
1.	0.148573	0.	0.148573	0.0831356	0.	0.083136
Fixed-Free (RR)						
0.2	0.	2.40391	0.841367	0.	0.703703	0.246296
0.4	0.061803	0.912745	0.930205	0.0271157	0.507542	0.4456
0.6	0.119107	0.458	0.587429	0.0667739	0.345961	0.360544
0.8	0.160391	0.19048	0.346859	0.104407	0.175304	0.243747
1.	0.16983	0.	0.16983	0.117445	0.	0.117445
Fixed-Free (CR)						
0.2	0.	4.0921	0.859341	0.	0.97809	0.205399
0.4	0.0363873	1.31565	0.63587	0.0135406	0.651832	0.270694
0.6	0.065964	0.579606	0.35827	0.0320575	0.410409	0.201147
0.8	0.0855798	0.221424	0.196001	0.0488009	0.196281	0.126471
1.	0.0906329	0.	0.0906329	0.0550073	0.	0.055007
Fixed-Fixed (RR)						
0.2	0.	1.43944	0.503805	0.	0.583116	0.204091
0.4	0.0336839	0.441821	0.487506	0.0204403	0.349923	0.324466
0.6	0.0540791	0.112018	0.233139	0.0423993	0.150092	0.20458
0.8	0.0480896	-0.0913073	0.0520515	0.0451544	-0.0540899	0.05995
1.	0.	-0.241079	-0.0843776	0.	-0.259465	-0.09081
Fixed-Fixed (CR)						
0.2	0.	1.93461	0.406268	0.	0.740211	0.155444
0.4	0.0156845	0.495142	0.258976	0.00925626	0.401921	0.175875
0.6	0.0235907	0.0868721	0.102842	0.0182717	0.145911	0.096166
0.8	0.0198757	-0.12552	0.0083622	0.0185957	-0.0798251	0.015722
1.	0.	-0.265242	-0.0557008	0.	-0.285628	-0.05998

Table 12. The present results for a hyperbolic disk subjected to internal/external pressures for $\beta_1 = \beta_2 = 1.5,\ -1.5$ $(p_a / p_b = 10)$.

r/b	u_r / b	σ_r / p_a	σ_θ / p_a	u_r / b	σ_r / p_a	σ_θ / p_a
	$\beta_3 = 0.75$ **(Divergent)**			$\beta_3 = -0.75$ **(Convergent)**		
$\beta_1 = \beta_2 = 1.5$						
Free-Free (RR)						
0.2	0.0714965	-1.	0.289484	0.138214	-1.	0.886227
0.4	0.00717797	-0.26151	-0.00073368	0.0465988	-0.445131	0.433637
0.6	-0.00180413	-0.141941	-0.0776287	0.0259035	-0.261857	0.309645
0.8	-0.00475526	-0.108954	-0.123198	0.0180423	-0.16475	0.265089
1.	-0.00621209	-0.1	-0.159242	0.0143738	-0.1	0.252477
Free-Free (CR)						
0.2	0.0411017	-1.	0.0105746	0.130743	-1.	0.491643
0.4	0.0021247	-0.308544	-0.0486689	0.0693615	-0.560769	0.408656
0.6	-0.00400879	-0.16988	-0.0729371	0.0519716	-0.35018	0.409547
0.8	-0.00600296	-0.121233	-0.0898893	0.0445673	-0.209202	0.434414
1.	-0.00690051	-0.1	-0.103806	0.0408683	-0.1	0.46942
$\beta_1 = \beta_2 = -1.5$						
Free-Free (RR)						
0.2	0.00117623	-1.	0.965063	0.00290949	-1.	2.90291
0.4	0.	-0.242908	-0.0868015	0.0015442	-0.154686	0.25106
0.6	-0.00095663	-0.152816	-0.122097	0.000755598	-0.0973045	0.020136
0.8	-0.00201421	-0.118939	-0.112002	-0.00013337	-0.0940659	-0.03758
1.	-0.00324082	-0.1	-0.0998165	-0.00135894	-0.1	-0.06218
Free-Free (CR)						
0.2	0.000452531	-1.	0.0935673	0.00394463	-1.	2.43614
0.4	-0.00033700	-0.328524	-0.108954	0.00286678	-0.203375	0.29725
0.6	-0.0010713	-0.189922	-0.085985	0.00216297	-0.122636	0.067326
0.8	-0.00183061	-0.131757	-0.0660444	0.00144753	-0.104818	0.008333
1.	-0.00262732	-0.1	-0.0525279	0.000592081	-0.1	-0.01390

Table 13. The elastic fields in a polar orthotropic hyperbolic disk subjected to internal/external pressures ($\beta_1 = \beta_2 = 0, \quad p_a / p_b = 10$) .

r / b	u_r / b	σ_r / p_a	σ_θ / p_a	u_r / b	σ_r / p_a	σ_θ / p_a
	$\beta_3 = 0.75$ **(Divergent)**			$\beta_3 = -0.75$ **(Convergent)**		
Free-Free (RR)						
0.2	0.00951039	-1.	0.601039	0.0211356	-1.	1.76356
0.4	0.001058	-0.243376	-0.0322819	0.00973399	-0.265654	0.393721
0.6	-0.0016937	-0.143157	-0.106562	0.00569615	-0.14438	0.139339
0.8	-0.00337936	-0.113077	-0.124061	0.00332975	-0.110034	0.0447317
1.	-0.00469782	-0.1	-0.128956	0.0015353	-0.1	-0.0042940
Free-Free (CR)						
0.2	0.0049135	-1.	0.0848101	0.0251418	-1.	1.29851
0.4	-0.00040061	-0.312134	-0.0775664	0.0167633	-0.347848	0.429851
0.6	-0.00243081	-0.178059	-0.0860086	0.0131127	-0.1936	0.221599
0.8	-0.003628	-0.126548	-0.080995	0.0109181	-0.131533	0.13615
1.	-0.00447595	-0.1	-0.0747114	0.00938474	-0.1	0.0916169

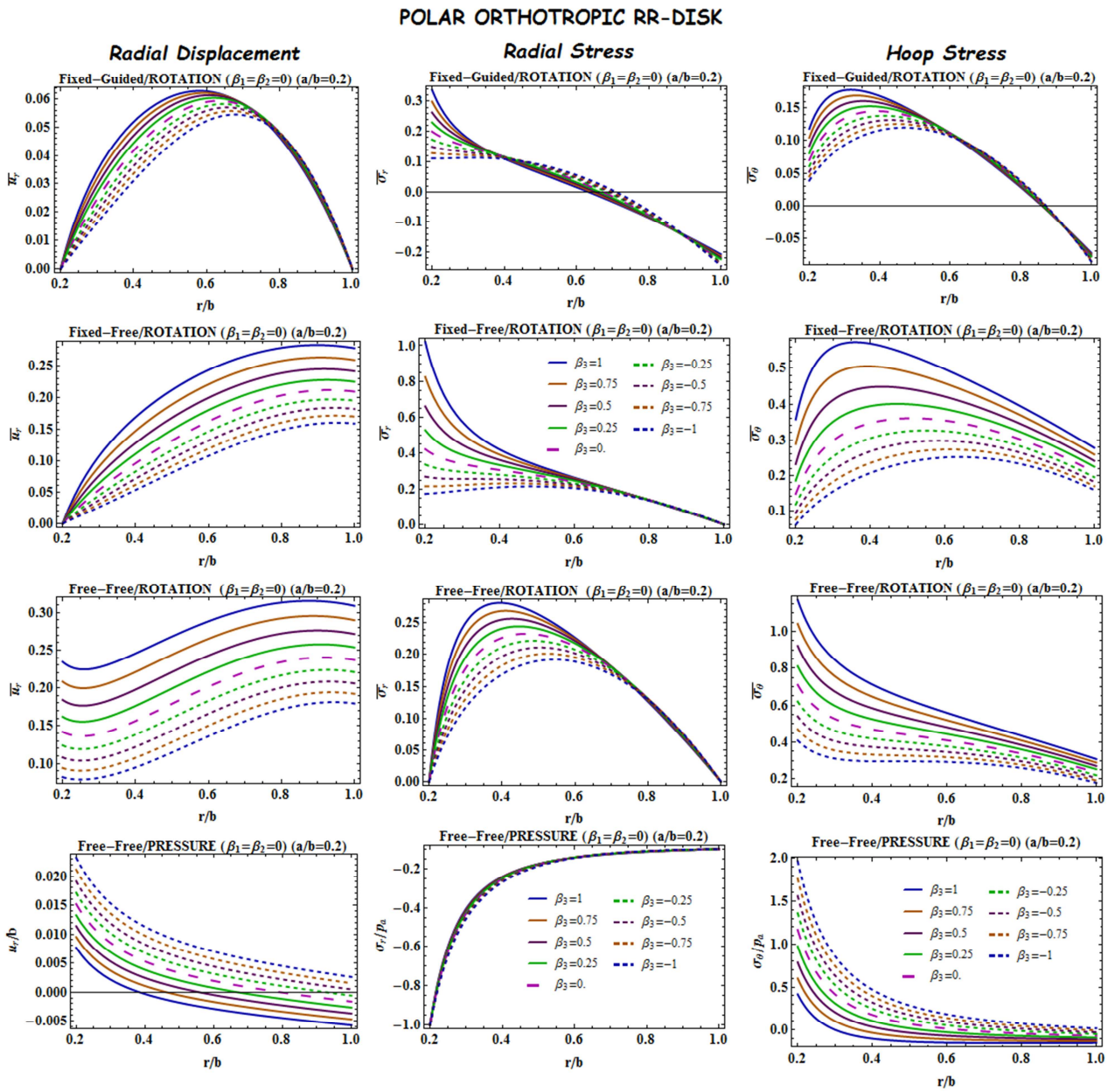

Figure 15. Variation of the elastic fields with the profile parameters in RR polar orthotropic hyperbolic disk.

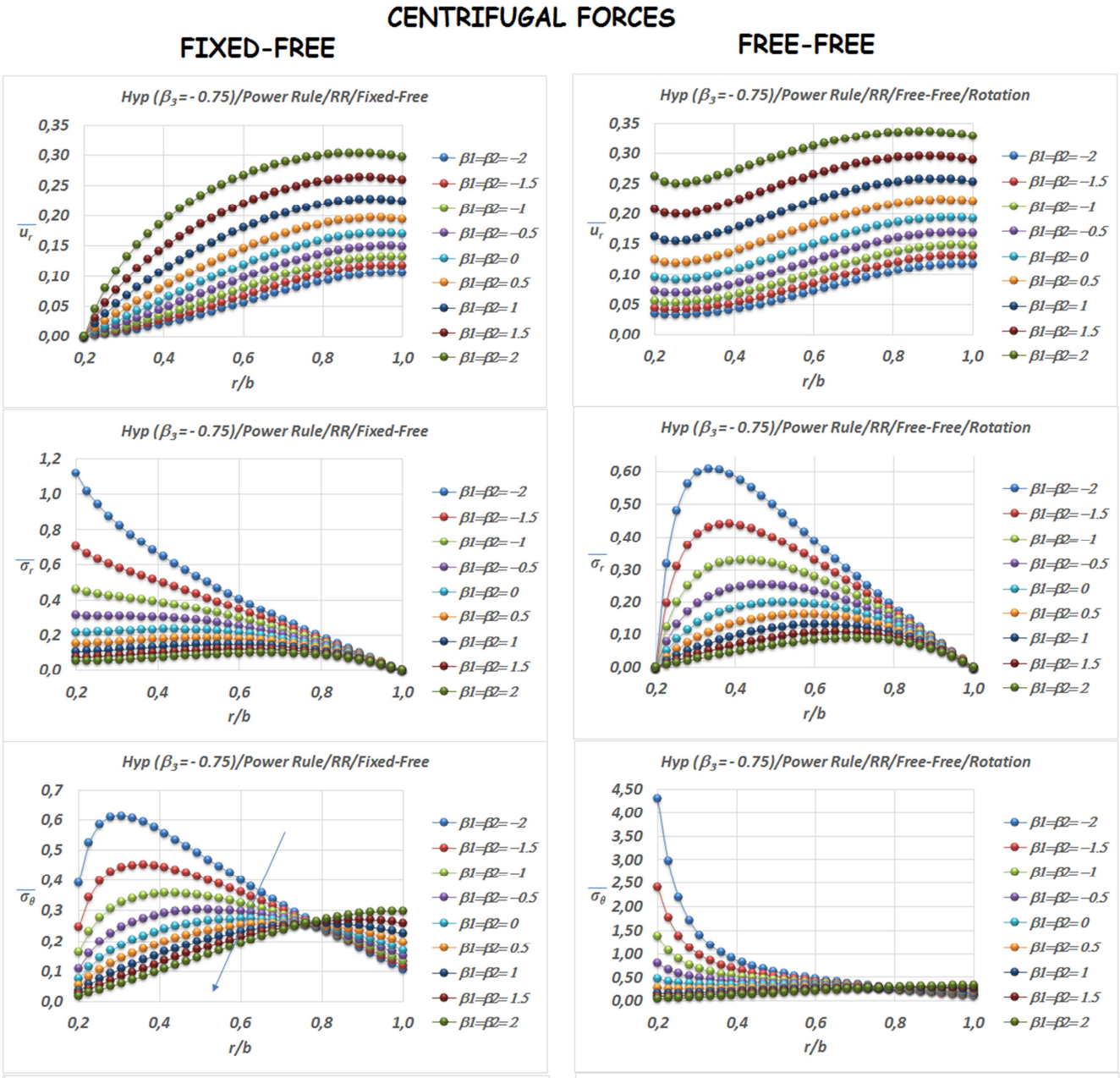

Figure 16. Variation of the elastic fields with the gradation parameter in convergent RR hyperbolic rotating disks under fixed-free and free-free boundary conditions.

Table 14. The elastic fields in a polar orthotropic hyperbolic disk subjected to centrifugal forces.

r/b	$\overline{u_r}$	$\overline{\sigma_r}$	$\overline{\sigma_\theta}$	$\overline{u_r}$	$\overline{\sigma_r}$	$\overline{\sigma_\theta}$
	$\beta_3 = 0.75$ **(Divergent)**			$\beta_3 = -0.75$ **(Convergent)**		
Free-Free (RR)						
0.2	0.208435	0.	1.04217	0.094261	0.	0.471305
0.4	0.22116	0.268937	0.647029	0.107816	0.182689	0.333481
0.6	0.26511	0.224698	0.520495	0.150526	0.195537	0.319314
0.8	0.292281	0.12798	0.410144	0.185629	0.13041	0.277679
1.	0.28982	0.	0.28982	0.192386	0.	0.192386
Free-Free (CR)						
0.2	0.263237	0.	1.31619	0.11909	0.	0.595448
0.4	0.254251	0.326142	0.704116	0.118871	0.226422	0.344726
0.6	0.265233	0.254731	0.495548	0.134381	0.227037	0.271646
0.8	0.271033	0.137592	0.367685	0.147074	0.143463	0.213969
1.	0.266212	0.	0.266212	0.148573	0.	0.148573
Fixed-Free (RR)						
0.2	0.	0.824348	0.288522	0.	0.215012	0.0752542

r/b	$\overline{u_r}$	$\overline{\sigma_r}$	$\overline{\sigma_\theta}$	$\overline{u_r}$	$\overline{\sigma_r}$	$\overline{\sigma_\theta}$
	$\beta_3 = 0.75$ **(Divergent)**			$\beta_3 = -0.75$ **(Convergent)**		
0.4	0.147407	0.391707	0.505616	0.061803	0.230908	0.235325
0.6	0.220417	0.258729	0.457917	0.119107	0.212859	0.273012
0.8	0.257589	0.137468	0.3701	0.160391	0.136297	0.248192
1.	0.258934	0.	0.258934	0.16983	0.	0.16983
Fixed-Free (CR)						
0.2	0.	1.77478	0.372703	0.	0.366008	0.0768618
0.4	0.108308	0.65816	0.408983	0.0363873	0.332836	0.160864
0.6	0.151422	0.355045	0.32693	0.065964	0.269377	0.166509
0.8	0.170208	0.1665	0.247725	0.0855798	0.158438	0.140247
1.	0.171352	0.	0.171352	0.0906329	0.	0.0906329
Fixed-Fixed (RR)						
0.2	0.	0.299156	0.104705	0.	0.128748	0.0450617
0.4	0.0495861	0.11327	0.16361	0.0336839	0.111773	0.12333
0.6	0.0621441	0.0210793	0.110951	0.0540791	0.0520611	0.108353
0.8	0.0471936	-0.0838949	0.0296287	0.0480896	-0.0653342	0.037245
1.	0.	-0.211994	-0.0741979	0.	-0.241079	-0.0843776
Fixed-Fixed (CR)						
0.2	0.	0.397566	0.0834888	0.	0.173037	0.0363377
0.4	0.0225922	0.114642	0.0805552	0.0156845	0.125262	0.0655163
0.6	0.0264682	-0.0006253	0.0439824	0.0235907	0.0403745	0.0477964
0.8	0.0190623	-0.10798	0.00115212	0.0198757	-0.0898149	0.0059835
1.	0.	-0.228594	-0.0480048	0.	-0.265242	-0.0557008

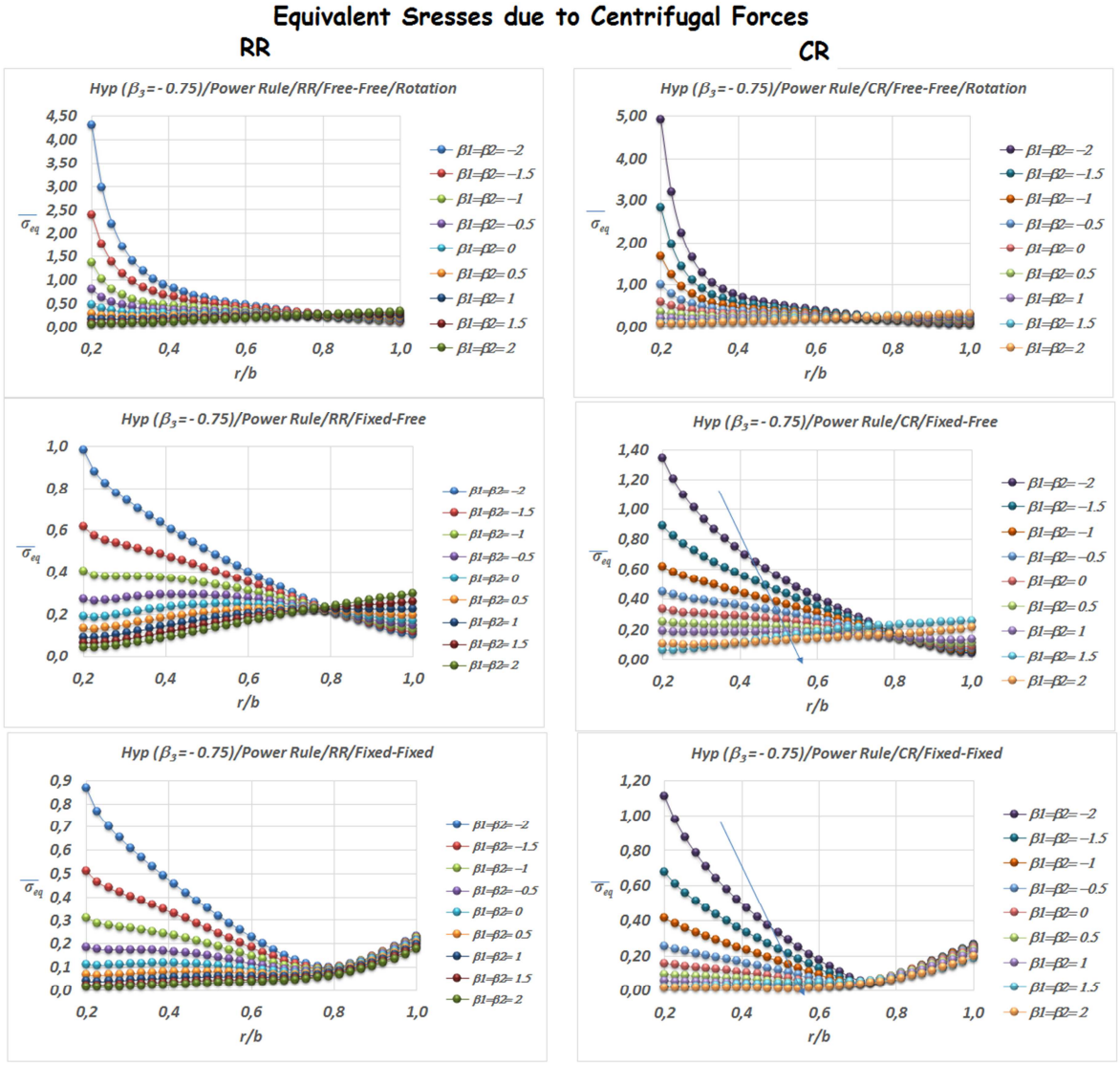

Figure 17. Variation of the equivalent stresses with the gradation parameter for convergent RR and CR hyperbolic rotating disks under three boundary conditions.

References

[1] Tang, S. 1969. Elastic stresses in rotating anisotropic discs, International Journal of Mechanical Sciences (IJMS), 11, pp. 509–517.

[2] Murthy, D. and Sherbourne, A. 1970. Elastic stresses in anisotropic discs of variable thickness, International Journal of Mechanical Sciences, 12, pp. 627-640.

[3] Reddy, T. Y. and Srinath, H. 1974. Elastic stresses in a rotating anisotropic annular disc of variable thickness and variable density, International Journal of Mechanical Sciences, 16 (2), pp. 85-89.

[4] Chang, C. I. 1974. A closed-form solution for an orthotropic rotating disc, Journal of Applied Mechanics, 41 (4), pp. 1122–1123.

[5] Chang, C. I. 1975. The anisotropic rotating discs, International Journal of Mechanical Sciences, 17 (6), pp. 397-402.

[6] Bert, C. W. 1975. Centrifugal stresses in arbitrarily laminated, rectangular-anisotropic circular discs, The Journal of Strain Analysis for Engineering Design, 10, pp. 84-92.

[7] Gurushankar, G. V. 1975. Thermal stresses in a rotating nonhomogeneous, anisotropic disc of varying thickness and density, The Journal of Strain Analysis for Engineering Design, 10, pp. 137-142.

[8] Christensen, R. M. and Wu. E. M. 1977. Optimal design of anisotropic (fiber-reinforced) flywheels, Journal of Composite Materials, 11, pp. 395-404.

[9] Belingardi, G., Genta, G. and Gola, M. 1979. A study of the stress distribution in rotating, orthotropic discs, Composites, 10 (2), pp. 77-80.

[10] Genta, G. and Gola, M. 1981. The stress distribution in orthotropic rotating discs, Journal of Applied Mechanics, 48, pp. 559-562.

[11] Jain, R., Ramachandra, K. and Simha, K. R. Y. 1999. Rotating anisotropic disk of uniform strength. International Journal of Mechanical Sciences, 41, pp. 639–648.

[12] Tutuncu, N. 2000. Effect of anisotropy on stresses in rotating discs, International Journal of Mechanical Sciences, 37, pp. 873–881.

[13] Zhou, F. and Ogawa, A. 2002. Elastic solutions for a solid rotating disc with cubic anisotropy, Journal of Applied Mechanics, 69, pp. 81-83.

[14] Callioglu, H. 2004. Stress analysis of an orthotropic rotating disc under thermal loading, Journal of Reinforced Plastics and Composites, 23 (17), pp. 1857–1869.

[15] Callioglu, H. 2007. Thermal stress analysis of curvilinearly orthotropic rotating discs, Journal of Thermoplastic Composite Materials, 20, pp. 357-369.

[16] Callioglu, H., Topcu M. and Altan, G. 2005. Stress analysis of curvilinearly orthotropic rotating discs under mechanical and thermal loading, Journal of Reinforced Plastics and Composites, 24, pp. 831-838.

[17] Callioglu, H., Topcu M. and Tarakçılar, A. R. 2006. Elastic-plastic stress analysis of an orthotropic rotating disc, International Journal of Mechanical Sciences, 48, pp. 985-990.

[18] Zenkour, A. M. and Allam, N. M. N. 2006. On the rotating fiber-reinforced viskoelastic composite solid and annular disks of variable thickness, International Journal of Computational Methods in Engineering Science and Mechanics, 7, pp. 21-31.

[19] Sayer, M., Topcu, M., Bektas, N. B. and Tarakcilar, A. R. 2005. Thermoelastic stress analysis in a thermoplastic composite disc, Science and Engineering of Composite Materials, 12 (4), pp. 251–260.

[20] Tahani, M., Nosier, A. and Zebarjad, S. M. 2005. Deformation and stress analysis of circumferentially fiber-reinforced composite disks, International Journal of Solids and Structures, 42 (9-10), pp. 2741–2754.

[21] Alexandrova, N. and Vila Real, P. M. M. 2008. Deformation and stress analysis of an anisotropic rotating annular disk, International Journal of Computational Methods in Engineering Science and Mechanics, 9 (1), pp. 43–50.

[22] Sen, F., Koruvatan, T. and Aldas, K. 2014. Thermal residual stresses in thermoplastic composite disc with holes using 3D-FEM, Advanced Composite Letters, 23 (4), pp. 79-87.

[23] Eraslan, A. N., Kaya, Y. and Varlı E. 2016. Analytical solutions to orthotropic variable thickness disk problems, Pamukkale University Journal of Engineering Sciences, 22 (1), pp. 24–30.

[24] Yıldırım, V. 2018. The complementary functions method (CFM) solution to the elastic analysis of polar orthotropic rotating discs. Journal of Applied and Computational Mechanics (JACM), DOI: 10.22055/JACM.2017.23188.1150 (in press).

[25] Horgan, C. and Chan, A. 1999. The pressurized hollow cylinder or disk problem for functionally graded isotropic linearly elastic materials, Journal of Elasticity, 55, pp. 43-59.

[26] Horgan, C. and Chan, A. 1999. The stress response of functionally graded isotropic linearly elastic rotating disks, Journal of Elasticity, 55, pp. 219-230.

[27] You, L. H. You, X. Y., Zhang, J. J. and Li, J. 2007. On rotating circular disks with varying material properties, Zeitschrift für angewandte Mathematik und Physik ZAMP, 58, pp. 1068–1084

[28] Bayat, M., Saleem M., Sahari B., Hamouda A., and Mahdi, E. 2008. Analysis of functionally graded rotating disks with variable thickness, Mechanics Research Communications, 35, pp. 283-309.

[29] Çallıoğlu, H., Bektaş, N. B. and Sayer, M. 2011. Stress analysis of functionally graded rotating discs: analytical and numerical solutions, Acta Mechanica Sinica, 27, pp. 950-955.

[30] Yıldırım, V. 2016. Analytic solutions to power-law graded hyperbolic rotating discs subjected to different boundary conditions, International Journal of Engineering & Applied Sciences (IJEAS), 8 (1), pp. 38-52.

[31] Yıldırım, V. 2017. Effects of inhomogeneity and thickness parameters on the elastic response of a pressurized hyperbolic annulus/disc made of functionally graded material, International Journal of Engineering & Applied Sciences, 9 (3), pp. 36-50. DOI: 10.24107/ijeas.329433

[32] Gang, M. 2017. Stress analysis of variable thickness rotating FG disc, International Journal of Pure and Applied Physics, 13 (1), pp. 158-161.

[33] Zenkour, A. M. 2005. Analytical solutions for rotating exponentially-graded annular disks with various boundary conditions, International Journal of Structural Stability and Dynamics, 5, pp. 557-577.

[34] Zenkour, A. M. 2007. Elastic deformation of the rotating functionally graded annular disk with rigid casing, Journal of Materials Science, 42, pp. 9717-9724.

[35] Argeso, H. 2012. Analytical solutions to variable thickness and variable material property rotating disks for a new three-parameter variation function, Mechanics Based Design of Structures and Machines, 40, pp. 133-152.

[36] Nejad, M. Z., Abedi, M., Lotfian, M. H. and Ghannad, M. 2013. Elastic analysis of exponential FGM disks subjected to internal and external pressure, Central European Journal of Engineering, 3, pp. 459-465.

[37] Nejad, M. Z., Rastgoo, A. and Hadi, A. 2014. Exact elasto-plastic analysis of rotating disks made of functionally graded materials, International Journal of Engineering Science, 85, pp. 47-57.

[38] Eraslan, A. N. and Arslan, E. 2015. Analytical and numerical solutions to a rotating FGM disk, Journal of Multidisciplinary Engineering Science and Technology (JMEST), 2 (10), pp. 2843-2850.

[39] Güven, U. 1995. Tresca's yield condition and the linear hardening rotating solid disk of variable thickness, Zeitschrift fur Angewandte Mathematik und Mechanik, 75, pp. 805-807.

[40] Zenkour, A. M. and Mashat, D. S. 2011. Stress function of a rotating variable-thickness annular disk using exact and numerical methods, Engineering, 3, pp. 422-430.

[41] Vivio, F., Vullo, V. and Cifani, P. 2014. Theoretical stress analysis of rotating hyperbolic disk without singularities subjected to thermal load, Journal of Thermal Stresses, 37, pp. 117–136.

[42] Eraslan, A. N. and Ciftci, B. 2015. Analytical and numerical solutions to rotating variable thickness disks for a new thickness profile, Journal of Multidisciplinary Engineering Science and Technology (JMEST), 2 (9), pp. 2359-2364.

[43] Vivio, F. and Vullo, V. 2007. Elastic stress analysis of rotating converging conical disks subjected to thermal load and having variable density along the radius, International Journal of Solids and Structures, 44, pp. 7767–7784.

[44] Vullo, V. and Vivio, F. 2008. Elastic stress analysis of non-linear variable thickness rotating disks subjected to thermal load and having variable density along the radius. International Journal of Solids and Structures, 45, pp. 5337–5355.

[45] Apatay, T. and Eraslan, A. N. 2003. Elastic deformation of rotating parabolic discs: analytical solutions (in Turkish), Journal of the Faculty of Engineering and Architecture of Gazi University, 18, pp. 115-135.

[46] Eraslan, A. N. and Akiş, T. 2006. On the plane strain and plane stress solutions of functionally graded rotating solid shaft and solid disk problems, Acta Mechanica, 181 (1–2), pp. 43–63.

[47] Hassani, A., Hojjati, M. H., Farrahi, G. and Alashti, R. A. 2011. Semi-exact elastic solutions for thermomechanical analysis of functionally graded rotating disks, Composite Structures, 93, pp. 3239-3251.

[48] Yıldırım, V. and Kacar, İ. 2017. Introducing a computer package program for elastic analysis of functionally graded rotating thick-walled annular structures, Digital Proceeding of ICOCEE – Cappadocia 2017, S. Sahinkaya and E. Kalıpcı (Editors), Nevsehir, TURKEY, May 8-10, pp. 1733-1742.

[49] Yıldırım, V. 2018. A parametric study on the centrifugal force-induced stress and displacements in power-law graded hyperbolic discs, Latin American Journal of Solids and Structures, LAJSS. (in press)

[50] Durodola, J. and Attia, O. 2000. Deformation and stresses in functionally graded rotating discs, Composites Science and Technology, 60, pp. 987-995.

[51] Chen, J., Ding H. and Chen W. 2007. Three-dimensional analytical solution for a rotating disc of functionally graded materials with transverse isotropy, Archive of Applied Mechanics, 77, pp. 241-251.

[52] Nie, G. J., Zhong, Z. and Batra, R. C. 2011. Material tailoring for orthotropic rotating disks, Composites Science and Technology, 71, pp. 406-414.

[53] Kansal, G. and Parvez, M. 2012. Thermal stress analysis of orthotropic graded rotating discs. International Journal of Modern Engineering Research (IJMER), 2 (5), pp. 3881-3885.

[54] Lubarda, V. A. 2012. On pressurized curvilinearly orthotropic circular disc, cylinder and sphere made of radially nonuniform material, Journal of Elasticity, 109, pp. 103-133.

[55] Peng, X. L. and Li, X. F. 2012. Elastic analysis of rotating functionally graded polar orthotropic discs, International Journal of Mechanical Sciences (IJMS), 60, pp. 84-91.

[56] Kacar, I., Yıldırım V. 2017. Effect of the anisotropy ratios on the exact elastic behavior of functionally power-graded polar orthotropic rotating uniform discs under various boundary conditions. Digital Proceeding of ICOCEE – Cappadocia 2017, Nevsehir, Turkey, pp. 1743-1752.

[57] Essa, S. and Argeso, H. 2017. Elastic analysis of variable profile and polar orthotropic FGM rotating disks for a variation function with three parameters, Acta Mechanica, 228, pp. 3877–3899.

[58] Zheng, Y., Bahaloo, H., Mousanezhad, D., Vaziri, A. and Nayeb-Hashemi, H. 2017. Displacement and stress fields in a functionally graded fiber-reinforced rotating disk with nonuniform thickness and variable angular velocity, Journal of Engineering Materials and Technology, 39, 031010-1-9.